1-1-1983

Analysis of near-millimeter waveguiding structures using surface magnetopiasmons.

Jean-Frederic O. Wagen

ANALYSIS OF NEAR-MILLIMETER WAVEGUIDING STRUCTURES USING SURFACE MAGNETOPLASMONS

by

Jean-Frederic O. Wagen

A Thesis

Presented to the Graduate Committee

of Lehigh University

in Candidacy for the Degree of

Master of Science

in Electrical Engineering

Lehigh University

1983

This thesis is accepted and approved
in partial fulfillment of the requirements
for the degree of Master of Science.

12/1/63
(date)

Professor in Charge

Chairman of Department

Acknowledgments

I would like to thank Professor Donald M. Bolle for his invaluable supervision and instructive guidance.

I am also indebted to Mrs Whei-Lin Hwang for the many constructive discussion throughout this work.

Table of Contents

LIST OF TABLE AND FIGURES

ABSTRACT

ANALYSIS OF NEAR-MILLIMETER WAVEGUIDING STRUCTURES
USING SURFACE MAGNETOPLASMONS

Together with the advantagious use in integrated circuit technology, doped semiconductors show interesting anisotropic characteristics under the application of a magnetic biasing field when exposed to electromagnetic excitations. Parameters can be chosen such that a near-millimeter wave interacts with the semiconducting material to exhibit non-reciprocal propagation. Such a behavior is considered in the fundamental case of the plane interface between dielectric and semiconductor regions to exploit the similarity in the field displacement effects of magnetoplasmons and edge-guided waves in ferrites (EGW). Subsequently, the curved single interface is analysed. The exact dispersion relation is derived and approximate expressions are given for the additional to the attenuation constant due to curvature effects. The last structure considered includes five regions defining two semiconducting slabs surrounded by dielectrics. The results of an exact analysis of the complex dispersion relation are given to provide the basic modal behavior. This is then used in the analysis of isolation and phase-shift capabilities.

TABLE I: LIST OF SYMBOLS

ω = angular frequency (rad/s)

$\omega_p = \sqrt{ne^2/\varepsilon_o m^*}$ (plasma frequency, rad/s)

$\omega_c = eB_o/m^*$ (cyclotron frequency, rad/s)

n = carrier concentration (m^{-3})

e = electron charge (coulombs)

m^* = electron effective mass (Kg)

= 0.067 m_e (for GaAs)

m_e = electron rest mass (Kg)

B_o = d.c. magnetizing field (web/m^2)

ε_o, μ_o = vacuum permittivity and permeability, respectively

$\varepsilon^{(o)}$ = static dielectric constant of the semiconducting material

= 12.95 (for GaAs)

$\nu = 1/\tau$ (collision frequency, rad/s)

τ = momentum relaxation time of the semiconducting material

$\gamma = \alpha + j\beta$ (complex propagation constant)

α = attenuation constant

β = phase constant

k_i = transverse wave number of the i-th region

ε_i = relative dielectric constant of the i-th region

$\varepsilon_e(\omega)$ = effective relative dielectric constant of the semiconducting medium ($\varepsilon_e(\omega) \equiv \varepsilon_2$)

D_1, D_2, D_3 = widths of the slab regions

1. INTRODUCTION

Increasing need for higher frequency bands in communication systems have led to the investigation of the near-millimeter wave range. Development of passive and active devices operating between K band and optical frequencies is aimed at yielding a very compact technology and large bandwidths. Thus, interests are in the analysis and design of non-reciprocal components which will perform, at high frequencies, the same important role as those already available at lower frequencies.

A promising technique, introduced by Nurmikko and Bolle in 1980, involves the use of surface waves supported by appropriate semiconducting substrates. The interaction of near-millimeter waves with the magnetically induced anisotropic properties of solid-state plasma leads to interesting non-reciprocal behavior that can be exploited in a number of useful devices.

The investigation of surface magnetoplasmons on high quality semiconductors have direct application to the design of isolators, phase-shifters, circulators, directional couplers and many other devices which will operate in the 100-1000 GHz range [1-5].

In this work, the basic structure considered is the interface between dielectric and semiconducting half-spaces. The unidirectionnal propagation of surface magnetoplasmons along such an

interface in a range of frequencies of interest to us, shows a similarity with the propagation of edge-guided wave (EGW) which occurs at lower frequency on ferrite microstrips [6]. With such a feature in mind, we first analyse the influence of several parameters on the propagation of surface magnetoplasmons along a flat single interface. Subsequently, the case of a curved interface is studied and expressions for bending losses are derived under the assumption of large radii and low material loss. Finally, a more complex structure is considered which involves two slabs of semiconductor surrounded by dielectric material delimiting four interfaces. The modal behavior is discussed and some dispersion and loss data are computed to provide information about the isolation and phase-shift capabilities. Only marginally acceptable characteristics are obtained principally due to material loss.

The substrate is presumed to be a high quality, moderately doped n-type GaAs material, with a carrier concentration of $n \cong 10^{15} cm^{-3}$ which is equivalent to a plasma frequency $\omega_p = 10^{13} rad/s$. At liquid nitrogen temperatures (77 K), mobilities of the order of $2 \times 10^5 cm^2/Vs$ which is equivalent to a momentum relaxation time of $8 \times 10^{-12} s$ can be obtained. Losses in the semiconductor are modelled through this parameter. The momentum relaxation time τ, which denotes the inverse of the collision frequency ν, represents the average time between collisions in the impurity scattering process. One can neglect both the interaction with lattice vibrations at

these low temperatures and the interaction with optical phonons due to the fact that our frequency range of interest is much less than the optical phonon frequency. Higher mobilities are also considered to provide numerical examples which apply to improved materials or techniques that are, however, not yet available.

For all the geometries considered, a biasing magnetic field is applied parallel to the interface(s) and perpendicular to the direction of propagation (Voigt configuration). A biasing magnetic field of 3810 Gauss which is equivalent to a cyclotron frequency $\omega_c=10^{12}$rad/s will generally be assumed. It should be pointed out that such a value satisfies the condition $\omega_c\tau>1$, which is required for an effective interaction between the semiconductor and the electromagnetic fields.

Under these circumstances and in the range of frequencies considered, the interaction is described well by the local theory of plasmas (Drude model). In this case the semiconducting material can be considered as an anisotropic dielectric medium characterized by a permittivity tensor $\underline{\underline{\epsilon}}(\omega)$ [2]. For a biasing magnetic field in the y-direction, the dielectric tensor takes the following form:

$$\varepsilon(\omega) = \begin{bmatrix} \xi & 0 & -j\eta \\ 0 & \zeta & 0 \\ j\eta & 0 & \xi \end{bmatrix} \qquad (1.1)$$

where

$$\xi = \varepsilon^{(0)} - \frac{\omega_p^2(\omega-j\nu)}{\omega[(\omega-j\nu)^2 - \omega_c^2]} \tag{1.2}$$

$$\eta = \frac{-\omega_p^2\omega_c}{\omega[(\omega-j\nu)^2 - \omega_c^2]} \tag{1.3}$$

$$\zeta = \varepsilon^{(0)} - \frac{\omega_p^2}{\omega(\omega-j\nu)} \tag{1.4}$$

and ω_c is the cylotron frequency,
ω_p is the plasma frequency
ν is tne collision frequency
ω is the operating frequency

See Table I for a complete list of symbols employed.

1.1 The plane semi-infinite structure

This case, represented in Figure 1.a, has already been studied in [2] and is restated here for the reader's convenience.

With no variation in the y-direction and assuming a uniform dc magnetic field B_o applied in this direction, the only solution that allows for transverse confinement in the vicinity of the interface is a TM mode: components H_y, E_x, E_z. It is assumed a propagation factor $\exp(j\omega t - \gamma z)$ where $\gamma = \alpha + j\beta$ is the propagation constant, solution of the dispersion relation (1.15). The electromagnetic fields distribution is then as follows.

-in the dielectric region (#1):

$$H_{y1} = A\, e^{k_1 x} \tag{1.5}$$

$$E_{x1} = \frac{1}{j\omega\epsilon_o\epsilon_1}\, A\, e^{k_1 x} \tag{1.6}$$

$$E_{z1} = \frac{k_1}{j\omega\epsilon_o\epsilon_1}\, A\, e^{k_1 x} \tag{1.7}$$

-in the semiconducting region (#2):

$$H_{y2} = A\, e^{-k_2 x} \tag{1.8}$$

$$E_{x2} = \frac{1}{j\omega\epsilon_o\epsilon_e}\left(\gamma - jk_2\frac{\eta}{\xi}\right) A\, e^{-k_2 x} \tag{1.9}$$

$$E_{z2} = \frac{-1}{j\omega\epsilon_o\epsilon_e}\left(k_2 + j\gamma\frac{\eta}{\xi}\right) A\, e^{-k_2 x} \tag{1.10}$$

where A is an arbitrary constant proportional to the square root of the power carried by the field (5.20) and $_e$ is the effective dielectric constant of the medium, given by:

$$\epsilon_e(\omega) = \frac{\xi^2 - \eta^2}{\xi} = \epsilon^{(0)}\, \frac{(\omega^2-\omega\omega_c-\omega_p^2/\epsilon^{(0)})(\omega^2+\omega\omega_c-\omega_p^2/\epsilon^{(0)})}{\omega^2(\omega^2-\omega_c^2-\omega_p^2/\epsilon^{(0)})} \tag{1.11}$$

The transverse decay factor satisfy:

$$k_1^2 = -\gamma^2 - k_o^2\epsilon_1 \tag{1.12}$$

$$k_2^2 = -\gamma^2 - k_o^2\epsilon_e \tag{1.13}$$

$$k_o^2 = \omega^2\mu_o\epsilon_o \tag{1.14}$$

Matching the boundary conditions at the interface gives the

following dispersion relation:

$$\frac{k_1}{\epsilon_1} = -\frac{k_2}{\epsilon_c} - \frac{j\gamma\cdot\eta}{\epsilon_e\cdot\xi} \qquad (1.15)$$

1.2 The edge guided waves

Within the frequency range ($\omega_1<\omega<\omega_6$ [1] and Fig.1.b) only the forward mode, called the S mode, may propagate. The fields distribution shows exponential decay on both sides of the interface with exponential decay factor k_i (region i). Thus it is readily seen that less than 1% of the amplitude of the fields remains beyond a distance greater than $5/k_i$ away from the interface into region i. Therefore, at any frequency between ω_1 and ω_6, the coupling between the two interfaces may be neglected if we consider a semiconducting slab wide enough (width $w>5/k_i$). Such slab forms a waveguide in which the fields cling to one interface in the forward direction of propagation and to the opposite for the reverse direction. This field displacement effect is quite similar to the one observed in the edge guided mode on ferrite microstrips [6]. Therefore, all the various structures envisaged for ferrite loaded devices such as circulators, isolators and phase-shifters using such modes can be transposed to the near-millimeter wave range. The conditions for such a transfer of device capabilities are that acceptable insertion loss must be obtained while attaining the required plasma concentration in the semiconducting material and for

structures of finite dimensions.

In this study we consider only the semi-infinite structure (no variation in the y-direction) and we refer to the H-guide described in [4] as an example of a more realistic geometry. Note that if contact injection is to be used for the the creation of the plasma concentration (see section 2.3 and [7]), the metal plates readily provide the necessary electrodes.

2. Influence of the parameters on the propagation

In the following we discuss the effects of:

- the dielectric loading (ϵ_1),
- the cyclotron frequency, proportional to the biasing magnetic field,
- the plasma frequency, related to the plasma concentration,
- and the collision frequency,

on the following propagation characteristics:

- attenuation constant (α),
- the exponential decay factors k_1 and k_2,
- and the useful bandwidth.

These parameters are of primary importance in our study since we seek devices that have low attenuation loss over large bandwidths. Furthermore, in our aim of designing non-reciprocal devices using the properties of dielectric-semiconducor interfaces, the transverse decay constants $d_i=1/Re[k_i]$ in the regions i (i=1,2) are important factors. Indeed, as explained in the introduction (1.2), the amplitude of the fields has decreased by more than 99% beyond $5d_i$ from the interface. Therefore the analysis for the plane single interface is still valid if another interface is placed at such a distance to form a slab waveguide or if the structure is curved by a radius of at least this order of magnitude. Section 3.3 gives more detail on this last point.

By defintion of $\omega_o^{(1)}$ (Figure 1.b and [1]), the effective permittivity ϵ_e is nul whon evaluated at this frequency. Thus, the dispersion relation (1.15) gives $k_2 = -j\gamma$. Therefore the transverse decay constant d_2 in the semiconducing region is seen to attain the value $1/\beta$ at $\omega_o^{(1)}$ and to asymptotically reach infinity at ω_6 since $k_2(\omega_6) = 0$ (Figure 1.b and [1]). Assuming a semiconducting slab with width w, each interface may be considered separately, i.e., with negligable coupling, for all frequency below ω_{max} such that $5d_2(\omega_{max})<w$. In this chapter, only slabs wide enough such that interface coupling can be ignore will be assumed.

2.1 Dielectric loading

To obtain meaningful insight into the effects of the dielectric loading (value of $_1$) the following parameters are plotted in Figure 3.

- d_1 : the transverse decay constant equal to the inverse of the exponential decay factor $Re[k_1]$ computed at ω_1 (Fig. 1.b). This frequency has been chosen since above it d_1 decreases, and only the forward mode propagates, as desired.

- $d(\omega_1)$: the attenuation constant computed at the same frequency as the one considered above. This factor strongly depends on the momentum relaxation time . Two cases ($\tau=8x10^{-12}$s and 10^{-10}s) have been considered giving an insight into the effects of available and improved material characteristics. In the case of $\tau=10^{-10}$s, a plot is also given for the attenuation constant evaluated at the upper frequency defined below. This provides the maximum value of the attenuation constant over the frequency range considered.

- BW : the useful bandwidth is defined in the lossless case

by $\mathrm{Min}(\omega_6,\omega_2)-\omega_1$ ([2], Fig.1.b). In the lossy case, BW is defined by $\omega_{up}-\omega_1$ where the upper frequency $_{up}$ is defined so that the insertion loss over a length equal of d_1 is constant. This definition is most meaningful when curved structures are considered. Indeed, in this case the dimension of the device is proportional to the radius and thus to d_1. Therefore the insertion loss in such a device, operating at the frequency , will be proportional to $\alpha(\omega)\cdot d_1(\omega_1)$. To obtain comparable results the insertion loss should remain constant. This constant, once chosen, allows computation of the upper operating frequency. In Figure 4, the constant is arbitrarily chosen to be equal to the value of the insertion loss defined in this way, at $\omega_0^{(1)}$ for $\epsilon_1=1$. This gives a value corresponding to an insertion loss of 3.9 db ($\tau=8\times10^{-12}$s) or .35 dB ($\tau=100\times10^{-12}$) over a length equal to $5d_1$ (1.7 mm).

As the dielectric loading increases, the energy on the dielectric side clings more to the interface as it is expelled from the dielectric medium. Thus, the transverse decay factor in the dielectric decreases and then, since more energy has to travel inside the semiconductor, the lossy material, the attenuation constant increases. Therefore a trade-off situation arises. The optimum dielectric loading with respect to these two factors (d_1 and α) can be found from the plot (Fig.3) of the product of these two parameters. However, the useful bandwidth has to be taken into account. Figure 3 shows that a relative permittivity of at least 4 is required to obtain interesting bandwidth characteristics. Since this value is near the optimum previously obtained and since the bandwidth requirement is to be emphasized, it follows that for the case considered, the optimum loading which minimizes the insertion loss for a structure of length proportional to d_1 and which maximizes the useful bandwidth is obtained for a dielectric of

relative permittivity equal to 4.

2.2 Cyclotron frequency

The cyclotron frequency ω_c is directly proportional to the amplitude of the biasing magnetic field through the relation (1.6). As a typical example a cylotron frequency of 10^{12}rad/s corresponds to biasing magnetic field of approximately 3810 Gauss.

The effect of the cyclotron frequency is studied by plotting (Fig.4):

- The transverse decay factor d_1 computed at the frequency ω_1.
- The attenuation constant α at this frequency.
- The useful bandwidth defined as in section 2.1. It is to be noted that the arbitrary constant has been chosen to be equal to 3 dB for $\tau=8\times10^{-12}$s.

As the cyclotron frequency, i.e., the biasing field, increases, it is observed (Figure 2.) that the effective permittivity increases quasi linearly, at least for some range of value. Therefore, as B_o increases more energy is expelled from the semiconductor into the dielectric region, thus the wave experiences lower loss and a higher value for the decay factor in the dielectric. However the trade-off situation obtained in the previous section does not appear here due to the sharp decrease in the attenuation constant. Indeed the product of these two factors, giving the insertion loss on a device of length d_1, decreases over the whole range of cyclotron

frequencies considered. In Figure 4. it is seen that to obtain a low attenuation constant the ratio ω_c/ω_p should be above 1/2. However, this is correct only for the attenuation constant computed at ω_1. In Figure 5, the attenuation characteristic is plotted with the cyclotron frequency as a parameter. It is then observed that a ratio ω_c/ω_p above .15 does not improve the loss figure further. Moreover, the useful bandwidth decreases above some value of ω_c/ω_p. Finally, to ensure a realistic value of the biasing magnetic field when the expected value of the plasma frequency is $\omega_p = 10^{13}$ rad/s, a ratio of 1/10 is chosen. This give a cyclotron frequency of $\omega_c = 10^{12}$rad/s (B_o=3810 Gauss).

2.3 Plasma and collision frequency

These parameters are generally determined by the semiconducting material considered. Here the effects of the plasma and collision frequencies are analysed to illustrate the desired characteristics of the semiconductor.

We rewrite the dielectric tensor elements (1.2) and (1.3) as:

$$\xi = \epsilon^{(0)} + \eta \frac{\omega - j\nu}{\omega_p} \left(\frac{\omega_c}{\omega_p}\right)^{-1}. \tag{2.1}$$

$$\eta = \frac{\omega_c/\omega_p}{\omega/\omega_p \left[(\omega - j\nu)^2/\omega_p^2 - \omega_c^2/\omega_p^2\right]} \tag{2.2}$$

It is readily seen that only the ratios ω_c/ω_p, ω/ω_p, ν/ω_p are involved. The choice of the plasma frequency is thus determined by the frequency range of interest and the available biasing magnetic field. To decrease the effect of material loss, a low ratio ν/ω_p is desired. Since the plasma frequency is proportional to the square root of the carrier concentration n and the collision frequency is inversely proportional to the mobility μ, the requirement for low loss is a high concentration n of carriers of high mobility μ. In a semiconductor, a large plasma concentration produced by doping means the introduction of impurities, thus increasing the plasma frequency also increases the collision frequency. Improved characteristics, compared to the one considered in this study, will be obtained if higher quality material can be produced or if more promising means for inducing plasmas than doping can be used in the present context of this study. Examples are contact injection, impact ionization, laser illumination. Further work in this direction is also suggested in section 4.3.

To give some insight into the dramatic improvement obtained from a higher collision frequency, the attenuation constants $\alpha(\omega_1)$ computed for $\tau = 8\times10^{-12}$s ($\nu = .125\times10^{12}$rad/s) and $\tau = 10^{-10}$s ($\nu = 10^{10}$rad/s) are plotted in Figure 3 (closely dotted lines).

2.4 Choice of the parameters

Generally, loss increases with the dielectric loading and decreases with increasing either the biasing field or the plasma frequency. The transverse decay factor in the dielectric region displays the opposite behavior, this is readily understood since loss occurs in the semiconducting material. The trade-off situation thus arising leads to slighlty different choices depending upon the particular applications and the required bandwidth.

Throughout the analysis of the five-region canonical structure the chosen parameters will then be the same as described in the introduction and the central dielectric will be chosen to have a permittivity four times that of vacuum.

Before studying such a structure, the aptitude of surface magetoplasmons in handling curvature is investigated. The curvature effects are of primary importance since curved structures are basic to EGW devices.

3. THE CURVED STRUCTURE

The effects of curvature on the propagation of surface waves along the interface between a dielectric medium and a semiconductor are investigated. Two possible geometries are represented in Figure 6.a and b, showing the cases where the center of curvature lies outside and inside the semiconducting region, respectively. Following the analysis given for the plane interface (1.1), we derive the dispersion relation for each structure. Due to the computational complexity of the analysis which involves Bessel functions, no attempt has been made here to obtain exact solutions. However, when large radii are considered, the propagation constants can be derived from those computed for the case of a plane interface. Furthermore, considering low material loss, the additional radiation loss introduced by the curvature can be obtained in a closed form following Marcuse's analysis [10]. The major assumption in this analysis is to consider a large radius R such that the field near the bent waveguide can be approximated by the field of the plane structure. Other methods include:

- the one presented by Marcatilli [11] which uses asymptotic formulae for Bessel functions to give an approximate form for the dispersion relation. This is then solved using the first terms of series expansions in 1/R.
- the perturbation method employed by Lewin [12]. His concern with circular waveguide did not allow the use of Marcuse's method due to the lack of any known solution of the wave equation in toroidal coordinates.
- the numerical method reported by Dang in a private

communication [ref.4 in [12]]. The case considered was a bent dielectric slab and Lewin pointed out that "since the propagation constant involves only a small imaginary part, very high accuracy in the computations is necessary for calculating the attenuation accurately".

The method presented by Marcuse has the advantage of simplicity while at the same time giving results which are in good agreement with those of Marcatilli. The disadvantage is the indeterminance of the range of validity of the formulae so derived. However the method is well suited for providing a first approximation of losses due to curvature.

3.1 Theory

In this section the field expression and the dispersion relations for the curved single interface are developed. The geometries considered are represented in Figures 6.a and b. These structures are assumed to be infinite in the y-direction. Note that the x and z coordinates are retained in the figures to indicates their correspondence to the cylindrical coordinates r and ϕ when R tends to infinity or R>>x. The TM modes interact with the anisotropic properties of the semiconductor polarized in the y-direction. These modes have three components: H_y, E_ϕ, E_r. The electric field components can be expressed as functions of the transverse magnetic field through Maxwell's equations. Assuming a propagation factor $\exp[j(\omega t - v\phi)]$, the wave equation in cylindrical coordinates becomes the well-known Bessel equation:

$$u^2 \frac{\partial^2 H_y}{\partial u^2} + u \frac{\partial H_y}{\partial u} + (u^2 - v^2) H_y = 0 \qquad (3.1)$$

where in the dielectric region:

$$u^2 = u_1^2 = k_o^2 \epsilon_1 r^2 \qquad (3.2)$$

or in the semiconductor:

$$u^2 = u_2^2 = k_o^2 \epsilon_e(\omega) r^2 \qquad (3.3)$$

Material loss in the semiconductor yields a complex effective permittivity written as:

$$\epsilon_e(\omega) = \epsilon_e'(\omega) - j\epsilon_e''(\omega) \qquad (3.4)$$

In this case u_1, u_2 and v are also complex and will be written as:

$$u_i = u_i' + j u_i'' \quad ; \; i=1,2 \qquad (3.5)$$

$$v = v' - j v'' = \beta_v R = \beta_c R - j\alpha_c R \qquad (3.6)$$

The general solution to the above equation (3.1) is a linear combination of Bessel functions of complex order v and complex argument u_i. The boundary conditions require bounded fields at the origin and at infinity. Considering the lossless case to simplify the initial analysis, the transverse magnetic field is found [13-15] to be respectively proportional to a Bessel function of the first kind and a Hankel function of the second kind. Using the following notation relating to the geometry of Figure 6.a,

$$\begin{aligned} F_v(u_1) &= J_v(u_1) \\ F_v(u_2) &= H_v^{(2)}(u_2) \end{aligned} \qquad (3.7)$$

and for the geometry of Figure 6.b,

$$F_v(u_1) = H_v^{(2)}(u_1)$$
$$F_v(u_2) = J_v(u_2) \tag{3.8}$$

and using the prime ' to denote the derivative with respect to the argument u_i, we obtain the following expressions for the fields valid in both geometries.

In the dielectric region:

$$H_{y1} = C\ F_v(u_1) \tag{3.9}$$

$$E_{\phi 1} = \frac{1}{j\omega\epsilon_o\epsilon_1}\frac{\partial H_{y1}}{\partial r} = \frac{C}{j\omega\epsilon_o\epsilon_1}\frac{u_1}{r}F_v'(u_1) \tag{3.10}$$

$$E_{r1} = \frac{1}{j\omega\epsilon_o\epsilon_1}\frac{1}{r}\frac{\partial H_{y1}}{\partial \phi} = \frac{C}{j\omega\epsilon_o\epsilon_1}\frac{jv}{r}F_v(u_i) \tag{3.11}$$

and in the semiconducting region,

$$H_{y2} = B\ F_v(u_2) \tag{3.12}$$

$$E_{\phi 2} = \frac{1}{j\omega\epsilon_o\epsilon_e}\left[\frac{\partial H_y}{\partial r} + j\frac{\eta}{\xi r}\frac{\partial H_y}{\partial \phi}\right] =$$

$$= \frac{B}{j\omega\epsilon_o\epsilon_e}\left[\frac{u_2}{r}F_v'(u_2) + \frac{\eta v}{\xi r}F_v(u_2)\right] \tag{3.13}$$

$$E_{r2} = \frac{-1}{j\omega\epsilon_o\epsilon_e}\left[\frac{1}{r}\frac{\partial H_y}{\partial \phi} - j\frac{\eta}{\xi r}\frac{\partial H_y}{\partial r}\right] =$$

$$= \frac{B}{j\omega\epsilon_o\epsilon_e}\left[\, j\frac{v}{r}F_v(u_2) + j\frac{\eta u_2}{\xi r}F_v'(u_2)\right] \tag{3.14}$$

where

$$u_1 = k_o\sqrt{\epsilon_1}\, r \tag{3.15}$$

$$u_2 = k_o\sqrt{\epsilon_e}\, r \quad \text{if } \epsilon_e'>0 \tag{3.16}$$

$$u_2 = -k_o\sqrt{\epsilon_e}\, r \quad \text{if } \epsilon_e'<0$$

This sign change is needed to ensure a finite field at infinity in the semiconductor. Another point of view could have been used when the real part of the effective permittivity is negative. We could then have considered the resulting Bessel equation as a modified Bessel equation whose solutions are written in terms of the modified Bessel functions. Such an approach would have lead to expression equivalent to (3.12)-(3.16) due to the relation between regular and modified Bessel functions [13,14].

It is found convenient to introduce the two positive quantities:

$$n_R = \sqrt{|\epsilon_e'|}\sqrt{\frac{1+\sqrt{1+(\epsilon_e''/\epsilon_e')^2}}{2}} \tag{3.17}$$

$$n_I = \frac{\epsilon_e''}{n_R} \tag{3.18}$$

and also the effective index of refraction n such that:

$$n = \sqrt{\epsilon_e} = n_R - j\, n_I \qquad \text{if} \quad \epsilon_e' > 0$$
$$n = -\sqrt{\epsilon_e} = n_I - j\, n_R \qquad \text{if} \quad \epsilon_e' < 0 \tag{3.19}$$

Applying continuity of the tangential field components at the interface (r=R) gives the relation between the amplitudes B and C and the dispersion relation:

$$C\, F_v(u_1) = B\, F_v(u_2) \tag{3.20}$$

$$\frac{u_1\, F_v'(u_1)/F_v(u_1)}{\epsilon_1} = \frac{u_2\, F_v'(u_2)/F_v(u_2)}{\epsilon_e} + \frac{\eta \cdot v}{\xi \cdot \epsilon_e} \tag{3.21}$$

with

$$u_1 = k_o \sqrt{\epsilon_1}\, R \tag{3.22}$$

and

$$u_2 = k_o\, n\, R \tag{3.23}$$

It is interesting to compare this dispersion relationship to the corresponding equation for the plane interface (1.15). It follows (see Appendix A.1):

$$\lim_{R\to\infty} [v/R] = \lim_{R\to\infty} [\beta_c] - j \lim_{R\to\infty} [\alpha_c] = -j\gamma = \beta - j\alpha \tag{3.24}$$

$$\lim_{R\to\infty} \left[\frac{u_i\, F_v'(u_i)/F_v(u_i)}{R}\right] = \begin{cases} k_1 = \sqrt{-\gamma^2 - k_o^2 \epsilon_1} & ;i=1 \\ k_2 = \sqrt{-\gamma^2 - k_o^2 \epsilon_e} & ;i=2 \end{cases} \tag{3.25}$$

3.1.1 Radius of curvature

In the case of the plane interface, the fields amplitude decays exponentially away from the interface with a constant decay factor k_i in the region i=1,2. Less than 1% of the field amplitude remains beyond a distance $d_i=5/Re[k_i]$ from the interface. Therefore if the radius of curvature R is greater than d_i, the effect of bending should be negligible. However, this is not the only condition. To neglect the effect of curvature, the radius must also be large enough so that the bend is negligible compared to the guide wavelength. It is assumed that over a distance of one guide wavelength, the curvature can be neglected if it introduces a deviation of less than 1% compared to the straight direction. This is illustrated by the following figure.

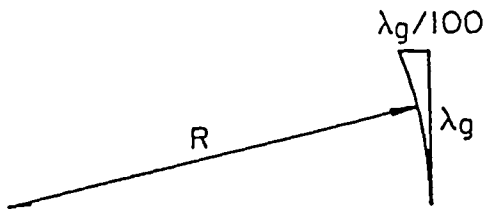

$$(R+\lambda_g/100)^2 \cong R^2 + \lambda_g^2 \quad ; \quad R \cong 50\cdot\lambda_g$$

Therefore the curvature effect may be neglected within approximately 1% error if the radius R satisfies the condition:

$$R > Max[\ 5/Re[k_i]\ ;\ 50\lambda_g\ ] \qquad (3.26)$$

At this point it is interesting to evaluate the order of magnitude involved in the above relations (3.21) and (3.26). For

this purpose we consider the following example:

$$\omega_p = 10^{13} \text{ rad/s} \quad ; \quad \epsilon^{(o)} = 13$$

$$\omega_c = 10^{12} \text{ rad/s}$$

$$\omega = 2.2\ 10^{12} \text{ rad/s} \quad = \quad 350 \text{ GHz}$$

Therefore $\xi = -13.04$, $\eta = -11.84$, $\epsilon_e = -2.29 < 0$ calculated here in the lossless case. For the plane interface case with $_1=1$, we compute for the S mode in the forward direction (section 1.1):

$$5/\mathrm{Re}[k_1] = 1.77 \text{ mm}$$
$$5/\mathrm{Re}[k_2] = .37 \text{ mm}$$
$$50\ \lambda_g = 40 \text{ mm}$$

and $k_o\sqrt{\epsilon_1}$ R = 15 R=2mm ; =300 R=40mm

$k_o\sqrt{|\epsilon_e|}$R = 22 R=2mm ; =440 R=40mm

R = 16 R=2mm ; =320 R=40mm

In the latter case (R=40mm) the asymptotic approximation for Bessel functions of large order and argument can be used to calculate the term involved in the dispersion relation (3.21). In this case, it can be shown (A.1.2) that the dispersion relation reduces to the one obtained for the flat interface case. As an example, the following relations are obtained in the case of Figure 6.a (5.18):

$$\frac{u_1}{R}\frac{J_\nu'(u_1)}{J_\nu(u_1)} = k_1 \cong 2822$$

$$\frac{u_2}{R}\frac{H_\nu^{(2)'}(u_2)}{H_\nu^{(2)}(u_2)} = k_2 \cong -13623$$

For the sake of simplicity the numerical value are given for the

lossless case.

In the case of a small radius (e.g. R=2mm), the computation of Bessel functions using the subroutine COMBES [16] gives:

$$\frac{u_1}{R}\frac{J_v'(u_1)}{J_v(u_1)} = k_1 \cong 3654$$

$$\frac{u_2}{R}\frac{H_v^{(2)'}(u_2)}{H_v^{(2)}(u_2)} = k_2 \cong -11426$$

This example shows that in the case of a radius larger than d_i but smaller than fifty times the guide wavelength, the curvature is non-negligible. Further work is needed if an exact propagation constant v is desired. In the following we will consider large radii such that the propagation constant v is related to the one computed for the flat interface through the relation (3.24): $v = \beta R - j\alpha R$. The attenuation constant (α) arises from the material loss and has to be increased by an additional term to account for the effects of curvature. This term is derived in the following section.

3.2 Bending loss

An approximate expression is derived for the attenuation constant α_{rc}. This gives the additional power loss due to curvature. The case of Figure 6.b is considered first for the lossless case. The analysis presented by Marcuse [10] is outlined. Then we consider the lossy case and finally formulae for the case of Figure 6.a are

given. This analysis has the main advantage that it shows clearly how radiation loss due to curvature arises. Indeed the field distribution, proportional to a Hankel function, is approximated by an asymtotic expression in which the radiation term is readily identified. Then the Poynting vector component due to such radiation is evaluated. Finally the power loss is calculated. It is pointed out that such calculation gives an expression for power loss due to the effects of curvature only. This term exists in both the lossless and lossy case. When the lossy case is considered, attenuation due to material loss is also to be taken into account. Therefore the total attenuation constant is given by a summation of the two contributions:

$$\alpha_{tot} = \alpha + \alpha_{rc} \tag{3.27}$$

3.2.1 Radiation in dielectrics: lossless case

The geometry considered is given in Figure 6.b. The field distribution can be represented by the transverse magnetic field H_y (section 3.1):

$$H_{y1} \sim H_v^{(2)}(k_o\sqrt{\epsilon_1}r)$$

Which is approximated in the case of large radii R as follows [13,14]:

$$H_{y1} = C\sqrt{\frac{1}{m\beta R}}\exp[\beta R(\operatorname{arctanh} m - m)] \tag{3.28}$$

where $m = \sqrt{1 - a^2 \frac{r^2}{R^2}}$ and $a = \frac{k_0\sqrt{\epsilon_1}}{\beta}$ (3.29)

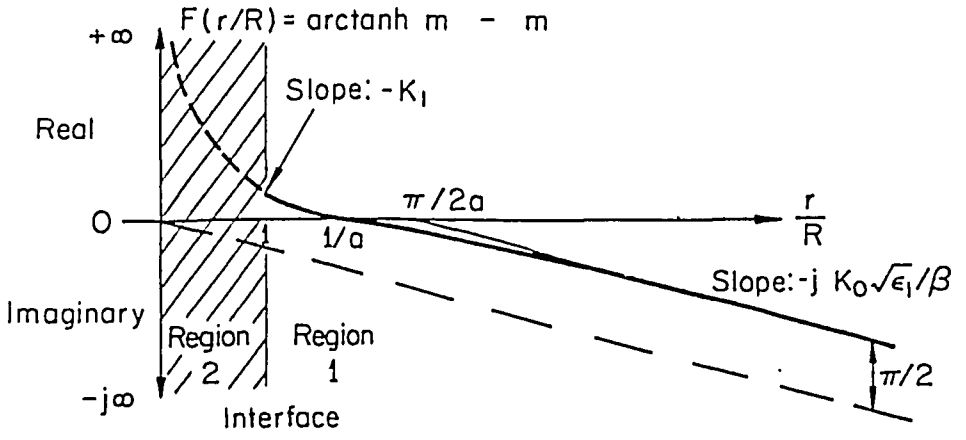

Figure 7 Exponent of (3.28)

This graph shows how the distribution of the fields (3.28) changes from a surface wave (5.14) at the interface ($r \cong R$) to an outward travelling wave (3.30) at the infinity (r approaching infinity) as the exponential factor $\beta \cdot R \cdot F(r/R)$ changes from real to imaginary values. Indeed as the ratio r/R is less than 1/a (3.29), the factor in the exponent of (3.28) is real and positive and its slope with respect to r is real and negative. This means that a certain value of $r/R < 1/a$, the first order expansion at this point shows that the amplitude of the fields decreases exponentially. As an example, near the interface ($r \cong R$; $r = R + x$, $x \ll R$), the expression for the transverse magnetic field can be approximated by (5.14) in which the term $\exp[-k_1 x]$ demonstrates the exponential decreasing behavior of the field distribution. It is to be pointed out that such distribution

is the same as for the plane case (1.5).

Above 1/a, the exponent of (3.28) becomes imaginary and for large value of r/R, H_{y1} becomes:

$$H_{y1} = C\sqrt{\frac{1}{k_o\sqrt{\epsilon_1}r}}\, e^{\{-jk_o\sqrt{\epsilon_1}r + j(v-1/2)\pi/2\}} \tag{3.30}$$

This expression demonstrates that radiation occurs in the dielectric region. We observe that (3.30) represents an outward travelling wave propagating in the positive r-direction in a medium of relative permittivity ϵ_1. The r-component of the Poynting vector is expressed using (3.30) and (3.10):

$$S = \mathrm{Re}[-1/2\ E_{\phi 1}H^*_{y1}]$$

$$S_r = \frac{1}{2}\frac{Z_o}{\sqrt{\epsilon_1}}\left|H_{y1}\right|^2 = \frac{C^2}{2\omega\epsilon_o\epsilon_1 r} \tag{3.31}$$

This expression represents the radial power flow at any angle ϕ. Each length element along the waveguide contributes an amount of radiated power proportional to the power carried by the mode, i.e., the ratio of the Poynting vector S_r to the power carried by the mode P is a constant with respect to ϕ. The value of this constant taken at the interface (r=R) gives the power loss $2\alpha_{rc}$ per unit length of waveguide.

$$2\alpha_{rc} = \frac{S_r(R)}{P} \tag{3.32}$$

Substitution of (3.31) and (A.25) into (3.32) yields:

$$2\alpha_{rc} = \frac{2k_1}{\epsilon_1}\left[\frac{\beta}{\epsilon_1 k_1} + \frac{\beta}{\epsilon_e k_2} - \frac{\eta}{\xi}\frac{1}{\epsilon_e}\right]^{-1} e^{-Re[U_1]\,R} \qquad (3.33)$$

with U_1 (A.15), a positive value which increases monotonically with frequency:

$$U_1 = 2\beta \operatorname{arctanh}\frac{k_1}{\beta} - 2k_1 \qquad ; \; k_1^2=\beta^2-k_o^2\epsilon_1$$

For constant radius, the power loss decreases as the frequency increases. Such behavior is to be expected since in this case the guide wavelength decreases, thus reducing the effect of curvature. It is also to be pointed out that if the dielectric permittivity increases, U_1 increases and so the power loss due to the curvature decreases, since the higher the dieletric constant, the more energy clings to the dielectric side of the interface and so the less radiation due to the curvature is likely to occur in the dielectric region.

3.2.2 Radiation in dielectric: lossy case

If material loss in the semiconductor is taken into account, the propagation constant v becomes complex (3.6). Since low loss is considered, only the factor in the exponent has to changed. The modified expression (3.31) of the r-component of the Poynting vector is:

$$S_r = \frac{C^2}{2\omega\epsilon_0\epsilon_1 r} e^{\alpha\pi R} e^{-2\alpha z} \qquad (3.34)$$

and the power loss due to curvature effect equals:

$$2\alpha_{rc} = \frac{2|k_1|}{\epsilon_1}\left[\frac{\beta}{\epsilon_1 k_1'} + \frac{\beta}{\epsilon_e' k_2} - \frac{\eta}{\xi\epsilon_e'}\right]^{-1} e^{\{-(\mathrm{Re}[U_1]-\alpha\pi)R\}} \qquad (3.35)$$

where only the real part of each parameters in the factor in front of the exponential need to be taken for the low loss case. This approximate formula shows how the material loss affects the bending loss, which not surprisingly increases as the attenuation constant of the corresponding plane structure increases.

3.2.3 Radiation in the semiconductor region

Two cases arise depending upon the sign of the real part of the effective permittivity. For the positive value, the case is much the same as the previous analysis, with ,however, some additional complexity due to the introduction of an imaginary part of the effective permittivity. The power loss is derived as before and using (5.36) takes the following approximate form:

$$2\alpha_{rc} = \frac{2|k_2|}{|\epsilon_e|}\left[\frac{\beta}{\epsilon_1 k_1'} + \frac{\beta}{\epsilon_e' k_2'} - \frac{\eta}{\xi\epsilon_e'}\right]^{-1} f_c\, e^{-(\mathrm{Re}[U_2]-\alpha\pi+2k_0 n_I)R} \qquad (3.36)$$

where

- $\epsilon_e' > 0$
- U_2 given by (A.15) can be rewritten:

$$U_2 = \beta \ln\{\mathrm{abs}[\frac{1+k_2/\beta}{1+k_2/\beta}]\} - 2k_2$$

If the real part of the effective permittivity is positive, i.e., for the frequency range between $\omega_o^{(r)}$ and ω_b, U_2 is also positive and decreases from infinity (in the lossless case) to zero as the frequency increases within this range. Therefore, R being constant, the power loss increases with frequency. This behavior is explained by the fact that the exponential factor in the semiconductor k_2 decreases with frequency, thus decreasing the energy on the semiconductor side of the interface.

- and where the amplitude factor f_c in (3.36) is a measure of α_{rc} and is given by:

$$f_c = \mathrm{Re}[\sqrt{|\epsilon_e|/\epsilon_e}]$$

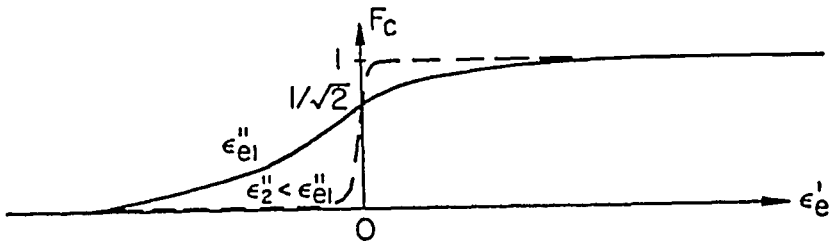

Figure 8 Factor f_c

It is interesting to note that for low loss, f_c tends to unity for positive values of the real part of the effective permittivity and thus does not alter the expression (3.36) dramatically. However, the exponent, when compared to the one in (3.35), has changed by a factor $2k_0n_IR$ where n_I is given by (3.18) and is proportional to the imaginary part of the effective permittivity. This factor conterbalances to some degree the effect of the attenuation constant

(α). This is intuitively correct since the radiation is absorbed by the lossy medium in which it occurs.

For negative values of the real part of the effective permittivity, the use of (5.37) in the previous analysis gives the following expression for the power loss:

$$2\alpha_{rc} = \frac{2|k_2|}{|\epsilon_e|}\left[\frac{\beta}{\epsilon_1 k_1'} + \frac{\beta}{\epsilon_e' k_2'} - \frac{\eta}{\xi\epsilon_e'}\right]^{-1} \cdot f_c \cdot e^{-(\mathrm{Re}[U_2]-\alpha\pi+2k_o n_R)R} \qquad (3.37)$$

where $\epsilon_e' < 0$.

In comparison with the previous case (3.36), this expression differs only by the change from n_I to n_R. Indeed in this case, radiation due to curvature effects occurs only due to material loss as can be seen from the radiation term $\exp[-jk_o n_I r]$ of the field distribution (5.32). It is in accordance with the expectation that the power loss in such a case increase with higher material loss as is shown by the behavior of the factor f_c. It is pointed out that the term $k_o n_R \cong K_o \sqrt{|\epsilon_e'|}$ in the exponent is somewhat compensated for by the term $k_2 \cong \sqrt{\beta^2 + k_o^2 |\epsilon_e'|}$ in $\mathrm{Re}[U_2]$. Also it can be seen that large negative values of ϵ_e' decrease, as expected, the power loss due to the factor f_c. In most cases the power loss given by (3.37) if found to be negligible. However, further work is needed to obtain a correct expression when the effective permittivity tends to zero.

3.2.4 Numerical examples

Let us consider a typical example:

$\epsilon_1=4$; $\epsilon^{(o)}=13$; $\omega_p=10^{13}$ rad/s; $\omega_c=10^{12}$ rad/s

Then at $\omega=2.4\text{x}10^{12}$ rad/s ($\cong$ 328 Ghz)

α =47 Np/m = .4 dB/mm if $\tau=10^{-10}$ s

β =19813 rad/m $50\lambda_g$=16 mm

k_1=11671 -j80 m^{-1} $5/\text{Re}[k_1]$=.43 mm

k_2=17106 +j95 m^{-1} $5/\text{Re}[k_2]$=.29 mm

Radiation into dielectric (Figure 6.b):

In the lossless case:

$\alpha_{rc}= 6259\ e^{-3454\ R}$ = .054 dB/mm (R=2mm)

and in the lossy case:

$\alpha_{rc}= 6259\ e^{-3306\ R}$ = .073 db/mm (R=2mm)

Radiation into semiconductor (Figure 6.a) : $\epsilon_e=1.56 > 0$

In the lossless case:

$\alpha_{rc}= 23528\ e^{-17558\ R} = 1.11\text{x}10^{-13}$ dB/mm (R=2mm)

and in the lossy case:

$\alpha_{rc}= 23505\ e^{-17410\ R} = 1.51\text{x}10^{-13}$ dB/mm (R=2mm)

At $\omega=2.2\text{x}10^{12}$ rad/s ($\cong$ 350 Ghz)

α =24 Np/m = .21 dB/mm if $\tau=10^{-10}$ s

β =16965 rad/m $50\lambda_g$=18.5 mm

$k_1 = 8510 - j49\ m^{-1}$ $\quad 5/\mathrm{Re}[k_1] = .59$ mm

$k_2 = 20287 + j89\ m^{-1}$ $\quad 5/\mathrm{Re}[k_2] = .25$ mm

Radiation into semiconductor (Figure 6.a) : $\epsilon_e = -2.30 < 0$

$\alpha_{rc} = 0$ in the lossless case

$\alpha_{rc} = 335\ e^{-60471\ R}$ negligible in the lossy case

at $\omega = 1.5 \times 10^{12}$ rad/s ($\cong$ 239 Ghz)

$\alpha = 4.3$ Np/m = .037 dB/mm if $\tau = 10^{-10}$ s

$\beta = 10455$ rad/m $\quad 50\lambda_g = 30$ mm

$k_1 = 3028 - j15\ m^{-1}$ $\quad 5/\mathrm{Re}[k_1] = 1.7$ mm

$k_2 = 26903 + j104\ m^{-1}$ $\quad 5/\mathrm{Re}[k_2] = .18$ mm

Radiation into dielectric (Figure 6.b):

In the lossless case:

$\alpha_{rc} = 860\ e^{-178\ R} = 5.2$ dB/mm (R=2mm)

In the lossy case:

$\alpha_{rc} = 860\ e^{-165\ R} = 5.4$ db/mm (R=2mm) lossy)

or $= .053$ db/mm (R=30mm)

Radiation into semiconductor (Figure 6.a) : $\epsilon_e = -24.5 < 0$

$\alpha_{rc} = 0$ in the lossless case

$\alpha_{rc} = 32\ e^{-43639\ R}$ negligible in the lossy case

These numerical examples show that bending loss in the semiconductor is negligible in the case of Figure 6.a and in the frequency range for which the effective permittivity is negative. Indeed, for these

frequencies the exponential decay factor k_2 in the semiconducting region is larger than the one in the dielectric region and thus the energy clings more tightly to the interface on the semiconductor side, thus being only weakly affected by the curvature. Bending loss in the case of Figure 6.b, i.e., radiation into the dielectric region due to curvature effects, could be non-negligible. A more accurate analysis should be undertaken if small radii are considered. However, for most cases power loss due to curvature effects can be neglected in the case of Figure 6.a and also in the case of Figure 6.b provided that large radii ($R>50\lambda_g$) are used here.

3.3 Range of validity

Difficulty arises when limits of validity have to be given for the relations developed. The three following criteria, ordered from the less to the most restrictive, have been encountered:

- $R > 5/Re[k_i]$; this essentialy allows us to ignore the effect of curvature on the transverse fields since their amplitudes decrease by more than 99% in the transverse direction for $r \tilde{=} R$ and if the analysis for the straight guide still holds.

- $R \gg R_{min}$ (5.38) ; this mathematical criteria is derived in appendix (I.4). It establishes the condition which allows the use of asymptotic expansions for the Bessel functions involved in the analysis. It leads to more severe conditions in the case of Figure 6.b. A more detailed analysis is needed for the special cases of nul or complex effective permittivities.

- $R > 50\lambda_g$; this criteria ensures that the curved structure may be approximated by the corresponding plane case, i.e. $v=\beta R$.

The given bending loss formulae hold for low material loss and large radii which satisfy these criteria. In this case and for the structure of Figure 6.b, the additional loss due to curvature has to be taken into account if the last condition is not respected. However, it can be neglected in the case of Figure 6.a or even in the case of Figure 6.b, provided that the third criterion is respected.

To conclude it is pointed out that interesting devices such as circulators, isolators, phase-shifters using edge wave-like surface magnetoplasmons should preferably be based on the structure represented in Figure 6.a where the curvature does not introduce excessive loss. Further work is needed to solve the dispersion relation more accurately and to allow extending such conclusions to the more general cases.

4. THE FIVE-REGION CANONICAL STRUCTURE

In this chapter a canonical structure of five regions including two slabs of semiconductors as shown in Figure 9.b is explored. The aim of this study is to provide the basic understanding of the modal behavior of such structures. This is the first step toward the study of devices such as isolators, phase-shifters, modulators, directional couplers. In the numerical analysis performed here, the case of opposed biasing fields in each slab is considered ($B_{04}= -B_{02}$). The chosen field amplitude corresponds to a cyclotron frequency $\omega_c=10^{12}$rad/s (B_0=3810 Gauss).

If the gap D_2 between the two semiconducting slabs is allowed to increase to infinity, it is seen that the dispersion characteristics must correspond to the case of the single semiconducting slab between dielectric material of the same (symmetrically loaded) or different permittivity (asymmetrically loaded, Figure 9.a). Considering a single slab of GaAs, the propagating waves exhibit a field displacement effect when exposed to a uniform d.c. magnetic field [1,2]. In addition, we observe non-reciprocal propagation characteristics for semiconducting slabs asymmetrically loaded. This is because, within the range of interest, the effective permittivity of the semiconductor becomes negative in two separate frequency intervals, i.e., for $0 < \omega < \omega_0^{(1)}$ and $\omega_\infty < \omega < \omega_0^{(2)}$, as seen in Figure 3 and further discussed in [1].

To remain in the lower frequency range, only the first interval is analysed. Thus, for a magnetized GaAs slab, only branches A and S (figure 10.a) are taken into account.

The theoretical analysis of the five-region canonical structure is briefly given in section 4.1 and follows closely the one given in [2], which can be considered as a particular case, i.e., no biasing field in the second semiconducing slab (region #4).

In section 4.2 the first results of this analysis are presented. Typical dispersion and loss diagrams are presented (Figures 11.,12.) and discussed.

4.1 Theory

The geometry to be analysed is shown in Figure 9.b. It is assumed to be infinite in the y-direction. Regions 1 and 5 extend to $x \rightarrow -\infty$ and $x \rightarrow \infty$ respectively. Regions 2 and 4 are the semiconducting slabs while region 1,3 and 5 are pure dielectric of any desired permittivity. The electromagnetic fields propagate in the z-direction.

For a uniform d.c. magnetizing field, the semiconductor is characterized by a permittivity tensors which takes the form given in the introduction (1.1). A subindex is added to indicate the region concerned. Only TM modes are considered here since fields

corresponding to TE modes do not exhibit interesting interactions with the semiconducting material. For an infinite structure in the y-direction only three field components results: H_y, E_x and E_z. The analysis is restricted to the bounded mode of the structure, i.e. those for which the field decays exponentially in the transverse direction, away from the guiding structure. For each region, the field component satisfies the wave equation obtained from Maxwell's equation. The solution for the transverse magnetic field H_y is obtained and the electric field components are then derived for each region to give:

-regions i = 1, 3, 5:

$$H_{yi} = A_i e^{k_i(x-x_i)} + B_i e^{-k_i(x-x_i)} \tag{4.1}$$

$$E_{xi} = \frac{\gamma}{j\omega\varepsilon_o\varepsilon_i}\left[A_i e^{k_i(x-x_i)} + B_i e^{-k_i(x-x_i)}\right] \tag{4.2}$$

$$E_{zi} = \frac{k_i}{j\omega\varepsilon_o\varepsilon_i}\left[A_i e^{k_i(x-x_i)} - B_i e^{-k_i(x-x_i)}\right] \tag{4.3}$$

-regions i = 2, 4:

$$H_{yi} = A_i e^{k_i(x-x_i)} + B_i e^{-k_i(x-x_i)} \tag{4.4}$$

$$E_{xi} = \frac{1}{j\omega\varepsilon_o\varepsilon_e}\left[(\gamma + jk_i\eta/\xi)\, A\, e^{k_i(x-x_i)} + (\gamma - jk_i\eta/\xi)\, B\, e^{k_i(x-x_i)}\right] \tag{4.5}$$

$$E_{zi} = \frac{1}{j\omega\varepsilon_o\varepsilon_e}\left[(k_i - j\gamma\eta/\xi)\, A\, e^{k_i(x-x_i)} - (k_i + j\gamma\eta/\xi)\, B\, e^{k_i(x-x_i)}\right] \tag{4.6}$$

In these relations,

$$K_i^2 = -\gamma^2 - K_0^2 \varepsilon_i \quad ; \quad i = 1,3,5 \tag{4.7}$$

$$K_i^2 = -\gamma^2 - K_0^2 \varepsilon_{ei}(\omega) \quad ; \quad i = 2,4 \tag{4.8}$$

$$K_0^2 = \omega^2 \mu_0 \varepsilon_0 \tag{4.9}$$

$$\varepsilon_{ei}(\omega) = \frac{\xi_i^2 - \eta_i^2}{\xi_i} \tag{4.10}$$

$x_1 = 0$

$x_3 = D_1$

$x_4 = D_1 + D_2$

$x_5 = D_1 + D_2 + D_3$

and A_m, B_m, $m = 1,\ldots,5$ are constants. Refer to Table I for a complete list of the symbols employed in these expressions.

The boundary conditions appropriate to the geometry represented in Figure 9.b, lead to a complex transcendental equation whose complex roots yield the propagation constants $\gamma = \alpha + j\beta$ characteristic of this waveguiding system. This transcendental equation or dispersion relation is given below. The notation employed is shown in Table I.

$$F(\omega,\gamma) = e^{-2K_2D_1} - \frac{e^{K_4D_3}(R_1 e^{K_3D_2} - R_2 e^{-K_3D_2}) - e^{-K_4D_3}(R_3 e^{K_3D_2} - R_4 e^{-K_3D_2})}{e^{K_4D_3}(R_5 e^{K_3D_2} - R_6 e^{-K_3D_2}) - e^{-K_4D_3}(R_7 e^{K_3D_2} - R_8 e^{-K_3D_2})}$$

$$F(\omega,\gamma) = 0 \tag{4.11}$$

The coefficients R_1 to R_8 are obtained from the function

$$\begin{aligned} R(u,k,v,e,m,n,p,q) = (K_4 + uj\gamma \frac{\eta_4}{\xi_4} + k\, \varepsilon_{e4} \frac{K_5}{\varepsilon_5}). \\ (K_4 + vj\gamma \frac{\eta_4}{\xi_4} + l\, \varepsilon_{e4} \frac{K_3}{\varepsilon_3}). \\ (K_4 + mj\gamma \frac{\eta_2}{\xi_2} + n\, \varepsilon_{e2} \frac{K_3}{\varepsilon_3}). \\ (K_4 + pj\gamma \frac{\eta_2}{\xi_2} + q\, \varepsilon_{e2} \frac{K_1}{\varepsilon_1}) \end{aligned} \tag{4.12}$$

in the following way

R_i = R(	u	k	v	l	m	n	p	q)
R_1 = R(	-1	1	1	1	-1	1	1	1)
R_2 = R(	-1	1	1	-1	-1	-1	1	1)
R_3 = R(	1	-1	-1	-1	-1	1	1	1)
R_4 = R(	1	-1	-1	1	-1	-1	1	1)
R_5 = R(	-1	1	1	1	1	-1	-1	-1)
R_6 = R(	-1	1	1	-1	1	1	-1	-1)
R_7 = R(	1	-1	-1	-1	1	-1	-1	-1)
R_8 = R(	1	-1	-1	1	1	1	-1	-1)

Throughout these calculations, a time dependence factor $e^{j\omega t}$ and a propagation factor $e^{-\gamma z}$ have been assumed. The dispersion

relation, when solved for different values of frequency , gives the modal spectrum of the configuration. Two typical examples are given in Figures 11 and 12. The dispersion relation is solved using an algorithm based on Davidenko's method [S.H. Talisa, Ph.D. dissertation, Brown University, June 1982]. This method consists of reducing the Newton-Raphson iterative procedure to a set of simultaneous first order differential equations in a dummy variable. This system is then solved numerically using the subroutine RKF 45 [3]. This algorithm has proven to be very efficient and reliable. The computations have been performed on the Hewlett-Packard 1000 of the Department of Electrical and Computer Engineering at Lehigh University. The program and its subroutines are written in FORTRAN language and is referenced under the filename SBGM6, a modified version of Talisa's SBGM3.

4.2 Results

Two typical loss and dispersion diagrams showing the lower modal spectrum for the five-region model considered are given in Figure 11 ($D_1=D_3=100\,\mu m$, $D_2=50\,\mu m$) and Figure 12 ($D_1=D_3=25\,\mu m$, $D_2=50\,\mu m$). As a first example, the case of two identical semiconducting slabs oppositely biased (i.e., $D_2=D_3$, $\epsilon_1=\epsilon_5$, $B_{02}=-B_{04}$) is considered. In the frequency range of interest, the dispersion diagram shows four possibles modes labeled O_S, E_S, O_A and E_A. This notation is used to refer to the odd and even distribution of the transverse magnetic field H_y. The subindices S and A refer to

the corresponding single slab case. Indeed the chosen geometry and biasing field polarisation lead to coupling between single slab modes which each show the same dispersion behavior. These single slab modes are labeled S and A to refer to the symmetric and antisymmetric distribution of the transverse magnetic field [1]. It is pointed out that because of our convention, the single slab dispersion diagram (Figure 10) for the reverse direction of propagation should be compared with the double slabs dispersion diagram (Figure 11, 12) for the forward direction and vice versa for the other direction of propagation. Due to the symmetry of the structure, the odd and even modes correspond to the case of a magnetic and electric wall respectively as a boundary condition in the middle of the central region (#3). Therefore the case of even modes has already been presented through the study of an "insulated image guide" [4]. This last structure has the advantage of decreasing the loss by half since only one lossy semiconducting slab is involved.

All the dispersion curves but E_A have the line k_0 as their low frequency asymptote. Near this asymptote, low loss as well as weak energy confinement is obtained. Another interesting feature is the turnback in the loss characteristic for the mode O_S and E_S, and also S in the single slab case. For the E_S and S cases this behavior can be explained by the following fact [1,2]: for some frequency range the fields adhere to one interface; as the frequency increases a

transition occurs in which the field energy is redistributed to the opposite interface. In the narrow frequency range over which this transition occurs, the attenuation constant increases considerably as more energy travels inside the GaAs slab, the only source of loss. Then the loss characteristics shows a lower loss region on a limited bandwidth before increasing again at high frequency as the mode becomes a "volume" mode for which the energy lies principally inside the semiconducting slab. For the O_S case, the turnback in the attenuation characteristic is due to radiation occurring in the vicinity of the cut-off frequency which is clearly defined for the lossless case only. A detailed explanation follows under the discussion of such a mode.

After these general statements, each mode is discussed in more detail.

E_A:

The dispersion curve of these modes starts, at low frequency, in the neighbourhood of the light line $k_0\sqrt{\epsilon^{(0)}}$ meaning that most of the energy travels inside the semiconducting slab. Then an asymptotic value given by the surface magnetoplasmon frequencies is approached as the propagation constant tends to infinity. In the case considered ω_{mp}=1.98 and 2.22 x10^{12}rad/s for the forward and reverse directions of propagation, respectively [1].

$$\omega_{mp} = \frac{\pm\omega_c + \sqrt{\omega_c^2 + 4\,\omega_p^2/(\epsilon^{(0)} + \epsilon_i)}}{2} \qquad (4.13)$$

i=1, $\epsilon_1 = 1$; ω_{mp} = 3.22 and 2.22 x10^{12} rad/s

i=3, $\epsilon_3 = 4$; ω_{mp} = 2.98 and 1.98 x10^{12} rad/s

At a given frequency the complex propagation constant for the reverse direction is always less than the value in the forward direction. Such non-reciprocal behavior increases with increased coupling, i.e., increase of the permitivitty of the central dielectric or decrease of its width D_2. Thus, this mode could have been promising for isolation or phase-shift purpose if its insertion loss had been lower (2-5dB/mm, 200-320GHz in the case of Figure 10). Using thinner semiconducting slabs increases the attenuation of this mode. This may be contrary to expectation. The reason for this behavior is that the A type modes experience a larger amount of energy travelling inside the semiconductor. Indeed, considering the single slab case, it is seen that as the width decreases, the coupling affects the dispersion curves in such a way that branch A moves further away from the dielectric light line, thus increasing the attenuation of this mode as more energy resides in the semiconducting slab. It is pointed out that S modes and its derivatives show the opposite behavior.

The E_A modes demonstrates the coupling effects. Indeed, considering branch A in the single slab case (Figure 10), it is seen

that the fields cling to the interface between the semiconductors and the dielectric of highest permittivity. The structure under study involves two such interfaces separated only by region 3 (width D_2), thus leading to a strong coupling. The coupling strengh is readily determined by the gap width D_2 and the dielectric permittivity of the central region (#3). Decreasing the dielectric region thickness by a factor 2 has approximately the same effect on the attenuation and dispersion curves as increasing the dielectric constant by a factor 4 [4].

O_A:

This mode is only slightly non-reciprocal. As its dispersion curve approaches the light line k_0, this mode is weakly confined. For example, in the case of Figure 11, at 240 Ghz, a 99% decrease in the field amplitudes is obtained about $3\lambda_g$ away from the "air-GaAs" interface, compared to $.8\lambda_g$ at the same frequency for the E_A mode. Its loss characteristics show attenuation increasing sharply as the dispersion curve moves away from the light line k_0. For the same example, attenuation less than 1 dB/mm is obtained below 320 GHz in the forward direction and below 290 GHz in the reverse direction. This shows that the O_A modes are useless for isolation.

The O_A mode does not show a cut-off frequency as could have been expected from the case of the odd mode on the corresponding symmetrically loaded dielectric slab [17]. The following facts

explain such absence. For the geometry considered, the central dielectric (region 3) can be seen as a symmetrically loaded dielectric slab with adjacent regions (1,2 and 4,5) corresponding to the surrounding medium in the symetrically loaded single dielectric slab case. At the interface between regions 2-3 and 3-4, the energy concentration begins to decrease as the frequency increases (note that for the 0_S mode the energy concentration increases with frequency). On the contrary, for the odd mode on a symetrically loaded single dielectric slab, the energy concentration at the interfaces increases with frequency. This explains why the cut-off pnenomena occurs for the 0_S mode only.

The weak non-reciprocity of the 0_A mode has been seen to be useless for isolation purpose. It is however sufficient to show weak differential phase-shift. The dispersion curves of the 0_A mode have been plotted in Figure 13 for several different geometries. It can be seen that such curves remain almost unchanged once the slab width ($D_1 = D_2$) exceeds about 100 μm. The explanation is obtained through the analysis of the field structure. When the dispersion curve is close to the light line k_0, the fields stick to the "external" interfaces, i.e., the interface between the regions 1-2 and 4-5. Once these two "external" interfaces are separated beyond a certain value, then no further influence is felt since the coupling between these two interfaces becomes negligible.

Since the 0_A mode derives from the A mode of the single semiconducting slab, the differential phase-shift increases as the non-reciprocity of this A mode increases. This is readily achieved by increasing the difference between the loading dielectric perimittivities, in the case considered $\epsilon_1 = \epsilon_5$ and ϵ_3, and decreasing the width of the semiconducting slab. Unfortunately, low insertion loss requires a large semiconducting slab width so that little energy travels in the central dielectric (region 3). Thus, a trade-off situation is met. To obtain the maximum differential phase-shift with an attenuation constant of less than 1 dB/mm, the following geometry has been chosen: $D_1 = D_3 = 200\,\mu m$; $D_2 = 25\,\mu m$. The differential phase shift is plotted versus the frequency in Figure 13. It is pointed out that the differential phase shift increases sharply with the frequency and simultaneously:

- the dispersion curve moves away from the light line k_0,
- the loss increases,
- the fields propagate more and more into the semiconducting slab to stick eventually to a new interface, i.e., the region 3-semiconductor interface.

In order to increase the differential phase-shift the following geometry has been tried : $D_1 = 100\mu m$; $D_2 = 50\mu m$; $D_3 = 25\mu m$. The aim was to obtain more non-reciprocity through an asymmetric structure. Results are given in Figure 13 and are found to be close to the ones previously plotted in the same figure.

The conlusion from this limited study of the 0_A phase-shift capability, is that hope of obtaining useful performance is subject to the premise of lower insertion loss.

E_S:

In the reverse direction of propagation, the dispersion diagram of this mode exhibits clearly the transition phenomena discussed in the introduction of this section. The loss characteristic follows the behavior previously described, but the lower attenuation constant reached in the turnback is still very large (9 dB/mm at 360 GHz, Figure 10). Meanwhile, in the forward direction, the geometry can be chosen such that the propagation experiences much lower loss, again at the cost of weaker energy confinement. In reference [4], where similar modes have been studied, an isolation ratio of 10:1 and insertion loss of less than .5 dB/mm over a bandwidth of 65 GHz in the 400 GHz range have been reported. In one of our example ,Figure 12, an isolation ratio greater than 30:1 and an insertion loss than 1 dB/mm over a 50 GHz bandwidth also in the 400 GHz is obtained. In this last example the field amplitudes decrease by more than 99% after $2.3\lambda_g$ at 414 GHz (worst case).

As explained in the beginning of this section, this mode has been discussed in [4] through the study of an "insulated image guide". Therefore, further information on this mode can be obtained from this reference.

O_S:

Unlike modes O_A, these modes are cut-off at a frequency which depends upon the geometry and upon the direction of propagation. This dependance is illustrated in Figure 14. The forward direction cut-off frequency is always lower than the one in the reverse direction. This is a promising feature for isolation purposes.

Recall that the cut-off frequency has been defined as the frequency at which the field amplitudes remain constant instead of decreasing exponentially away from the slabs: $k_1 = k_5 = 0$. In the reverse direction and as the frequency increases, the energy is closely restrained to the interfaces between the central dielectric and the semiconductor slabs. At the same time the propagation constant increases, ultimately becoming infinite as the frequency reaches a surface magnetoplasmon frequency ($\omega_{mp} = 2.98 \times 10^{12}$ rad/s for $\epsilon_3 = 4$). Therefore, the mode O_S exists only between these two limits; above the cut-off frequency and below that surface magnetoplasmon frequency. As the geometry changes with decrease in D_2 or in $D_1 = D_3$, the cut-off frequency increases. In the reverse direction and below a certain width $D_1 = D_3$ or gap D_2, the O_S mode ceases to exist since the cut-off frequency approaches the surface magnetoplasmon frequency. Numerically, problems arise near this condition due to conflicting requirements: one being $k_1 = 0$, the other $k_1 \rightarrow \infty$.

Another feature of 0_S modes is the turnback in the loss characteristic in the vicinity of the cut-off frequency. This is due to the conditions used to defined the cut-off frequency, which looses its strict meaning when loss is taken into account.

For isolation purposes, a narrow semiconducting slab should be used to lower the insertion loss but the bandwidth over which the insertion loss is acceptable (.5 or 1 dB/mm) decreases. With the following configuration: $D_1=D_2=D_3=50\mu m$ an infinite isolation ratio is obtained on a 31 (48) GHz bandwidth in the 400 GHz range with an insertion loss smaller than .5 (1.) dB/mm. Confinement (99% decrease in the field amplitude in the transverse direction) is never better than $4\lambda_g$ at 450 GHz and deteriorates as the frequency decreases toward the cut-off frequency. These results may be compared with the 65 GHz and 50 GHz bandwidth in the 400 GHz range, 10:1 isolation ratio, .5 dB/mm insertion loss obtained respectively for an insulated image guide [4] and a five-region canonical structure with only one semiconducting slab [2]. The advantage of the present structure resides mainly in the infinite isolation ratio due to the difference between the cut-off frequency in the forward and reverse directions.

Strange behavior occurs in the dispersion characteristic in the reverse direction for the cases shown in Figures 11 and 12 and in the forward direction in Figure 10. Such oddities are only present

in high loss ranges which are useless for any practical application. Furthermore, they disappear when loss is removed, thus decreasing interests in their study. However, it is worth noting that in the vicinity of the critical frequencies such as $\omega_1^{(0)}$ and ω_∞, the effective dielectric constant of semiconducting material presents a large imaginary part compared to its real part (Figure 2). In this case, the semiconductor appears as a lossy conductor which thus expels the energy instead of allowing its propagation. This fact, together with the coupling phenomena involved, could provide some insight into this behavior, but more data would be needed to achieve certainty. However, as previously stated, efforts in this direction have no practical interest since losses are excessive.

4.3 Suggestion for further work

From the observation of the dispersion and attenuation diagrams for all lower modes in both reverse and forward direction, it can be stated in general terms that acceptable loss (<1 dB/mm) can be obtained only at the expense of a somewhat weak confinement, on the order of several guide wavelength to obtain at least 99% decrease of the amplitude of the fields in the transverse direction. To improve non-reciprocal device capability over a specified bandwidth, the coupling between the two semiconducting slabs has to be increased. Unfortunately this also increases the insertion loss. A way to decrease the loss by half is to use an insulated image guide already discussed in [4], whenever only the even modes are considered.

Further works should include the investigation of the directional coupling capabilities of the structure considered. It is believed that the behavior of such a model will follow closely the simplified theory given in [3] where a five-region canonical structure with only one semiconducting slab was studied. Furthermore, the independance of the biasing fields open the possibility of interesting modal behavior that could be applied to the design of modulators, switches and directional couplers. However, it is pointed out that losses will remain an important problem as long as doping is used to obtain the required plasma concentration in the semiconducting materials.

As briefly stated in section 2.3, other means of inducing a solid-state plasma through impact ionization, contact injection and photon induced carrier creation have been described in [7]. The optical technique mainly offers the advantage of total electric isolation. High mobility and high carrier concentration leading to low loss effects may be achieved more readily through injected plasmas, since it involves both electrons and holes instead of only one type of carrier as is the case in doped material. Also, impurities introduced by the doping process are avoided, thus improving the loss figure. Although a number of millimeter wave devices use the conductive properties of optically produced solid-state plasmas [8,9], little information has been found on the practical utilization of its dielectric properties. From Mortenson

et al. [7], we understood that it is due to the extremely high magnetic fields or very low temperatures required. However, the structure considered here will achieve acceptable performance if the collision frequency can be decreased as is promised by injected plasmas. Further work is needed in this area.

5. CONCLUSION

In the aim of providing useful information for the design of near-millimimeter wave passive devices such as isolators, phase-shifters, circulators, two structures have been analysed which use the non-reciprocal properties of the propagation of surface magnetoplasmons on semiconducting substrates. The first structure is simply formed by two half-spaces, one dielectric, the other a semiconductor polarized by a biasing magnetic field. The unidirectional propagation over a certain frequency range can be exploited in schemes similar to the edge guided wave propagation [9]. This could allow the design of useful devices if material loss is reduced and if the unidirectivity property is conserved with small radii of curvature. Further work in this direction would require an accurate analysis of the dispersion relation in the case of small curvature.

More complex in terms of its geometry, the second structure includes two semiconducting slabs which in our numerical examples, are oppositely biased by a magnetic field. These two slabs are surrounded by dieletrics. The modal behavior is analysed and device capabilities including isolation and differential phase shift are found to be spoiled by excessive loss.

The material loss considered arises due to impurities in the

doped semiconductors. Doping is needed to achieve the required plasma concentration. Other mean such as contact injection, impact ionization, or laser illumination [7] seem promising since they induce carriers without disturbing the substrate composition. Further investigation is needed to prove the validity of such an approach.

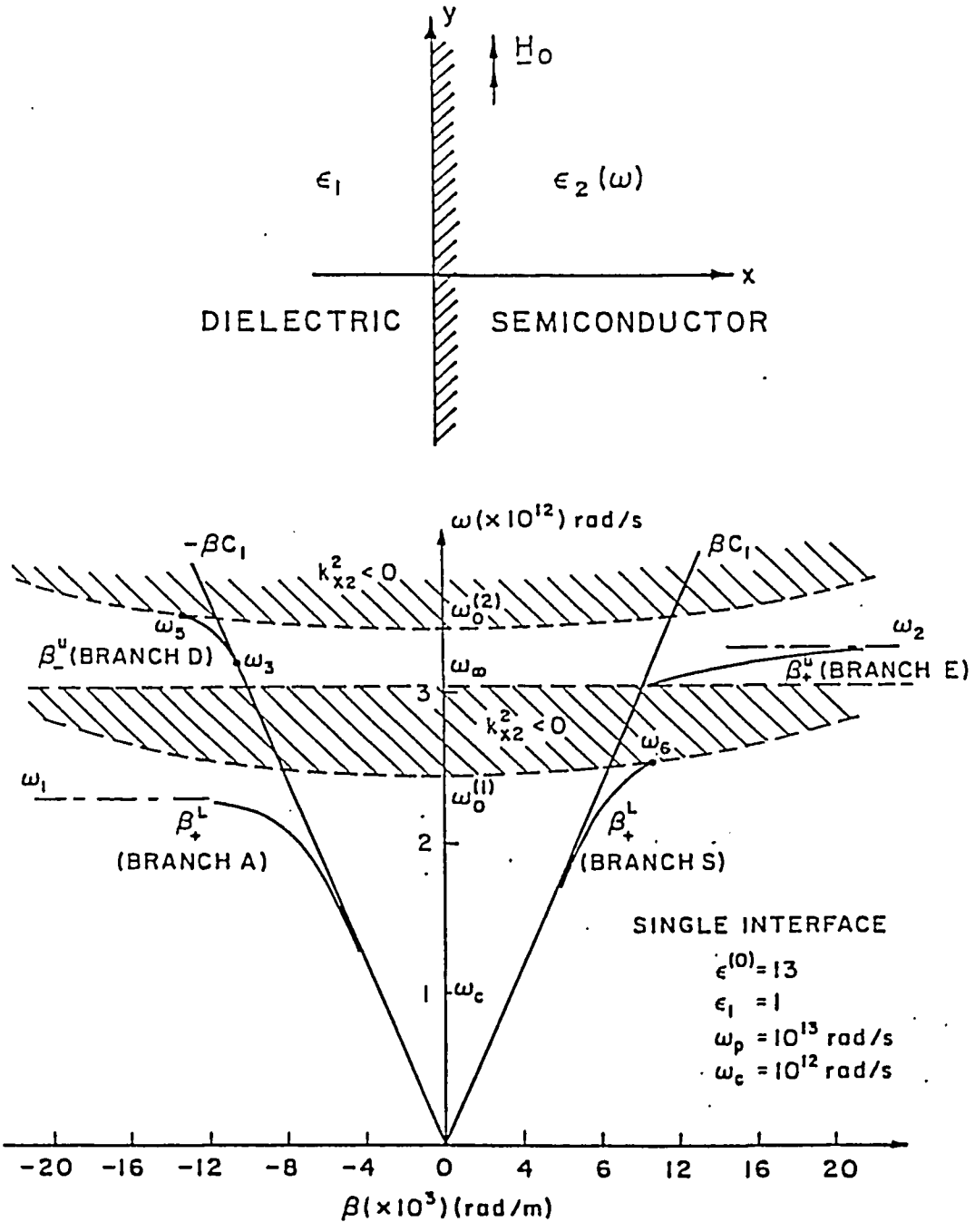

Figure 1.a Dielectric-semiconductor flat interface.
1.b Dispersion diagram. (After D.M. Bolle)

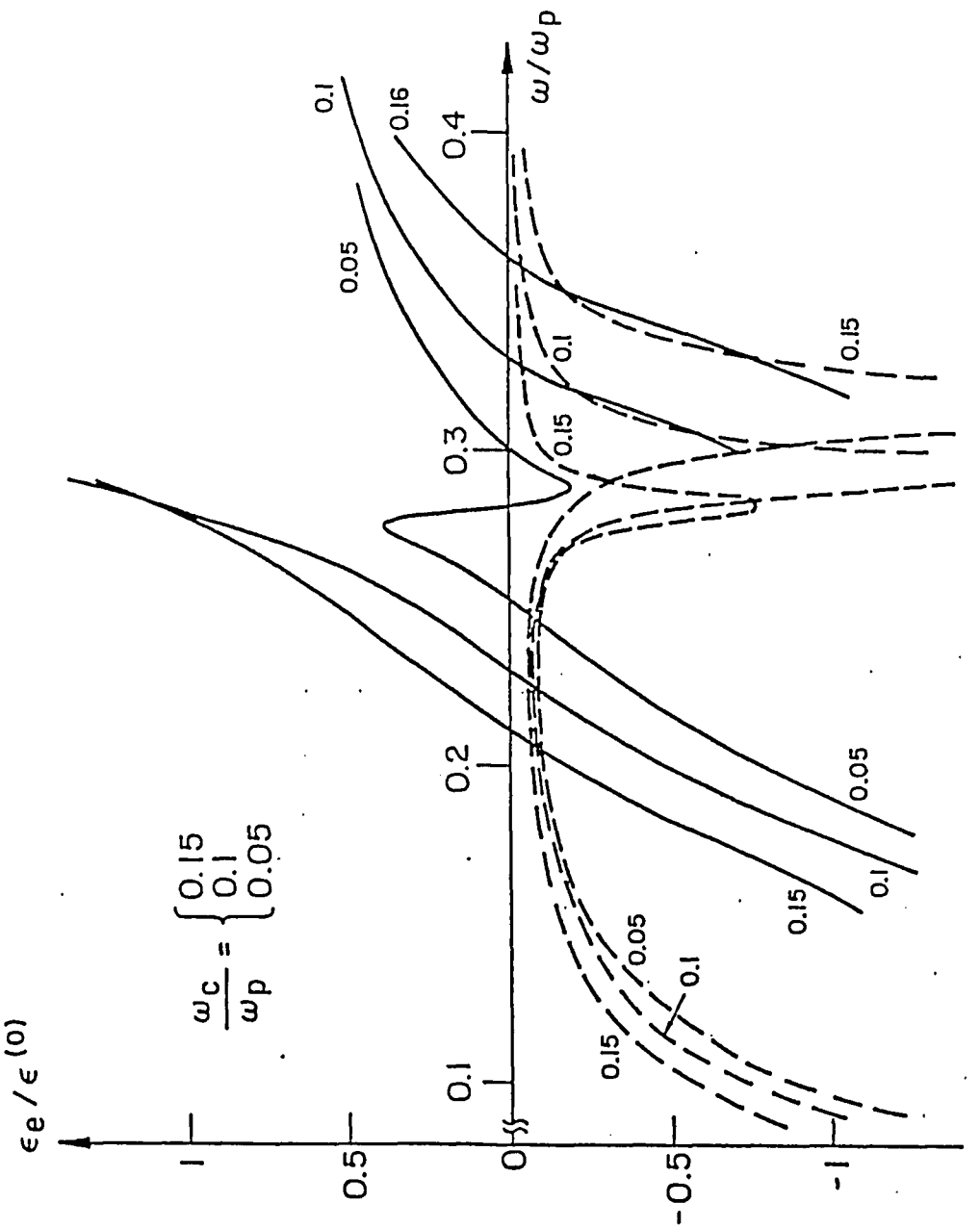

Figure 2 Real and imaginary parts of the effective dielectric constant for different values of ω_c. $\tau = 1/\nu = 8 \times 10^{-12}$s (After S.H. Talisa)

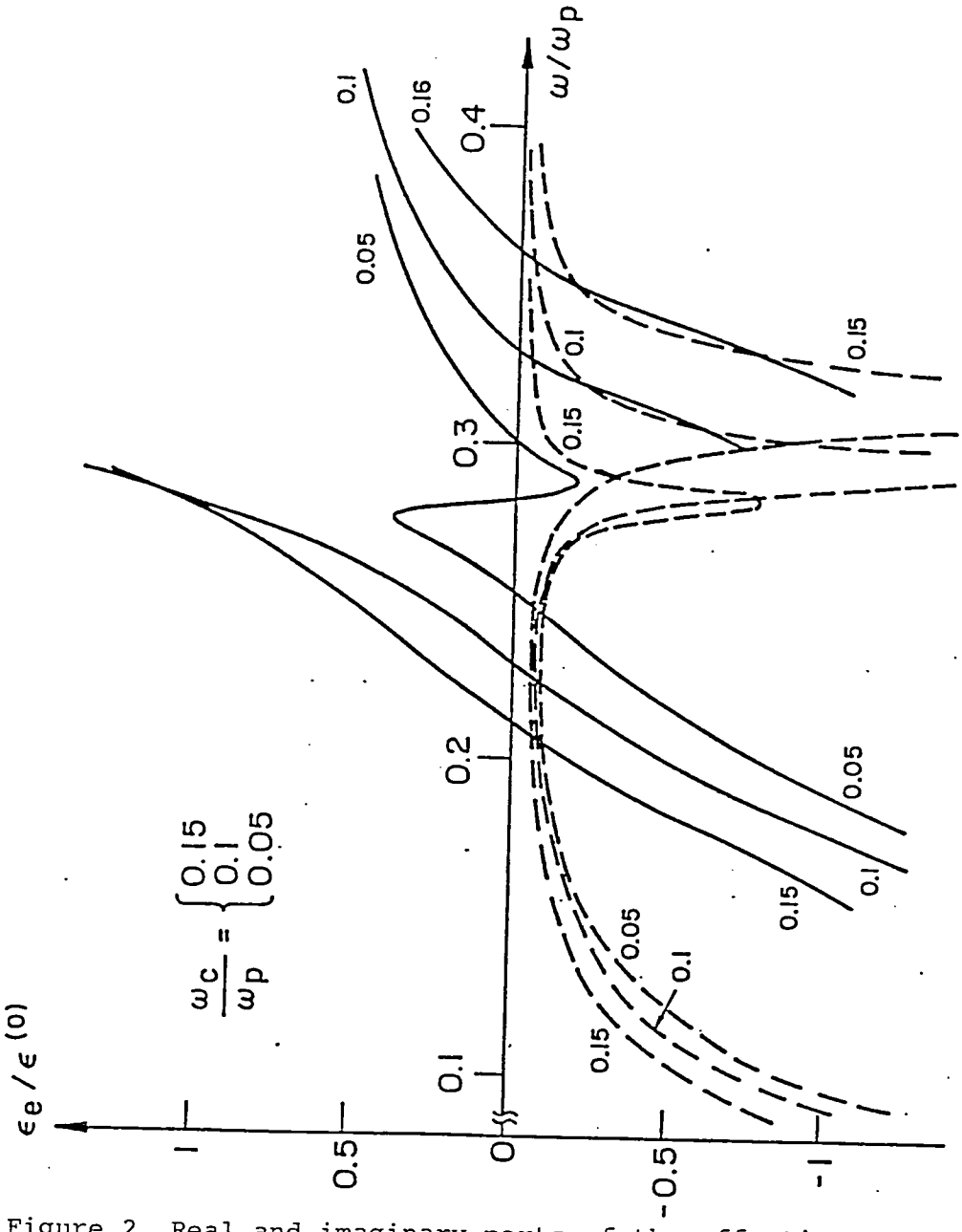

Figure 2 Real and imaginary parts of the effective dielectric constant for different values of ω_c. $\tau = 1/\nu = 8 \times 10^{-12}$s (After S.H. Talisa)

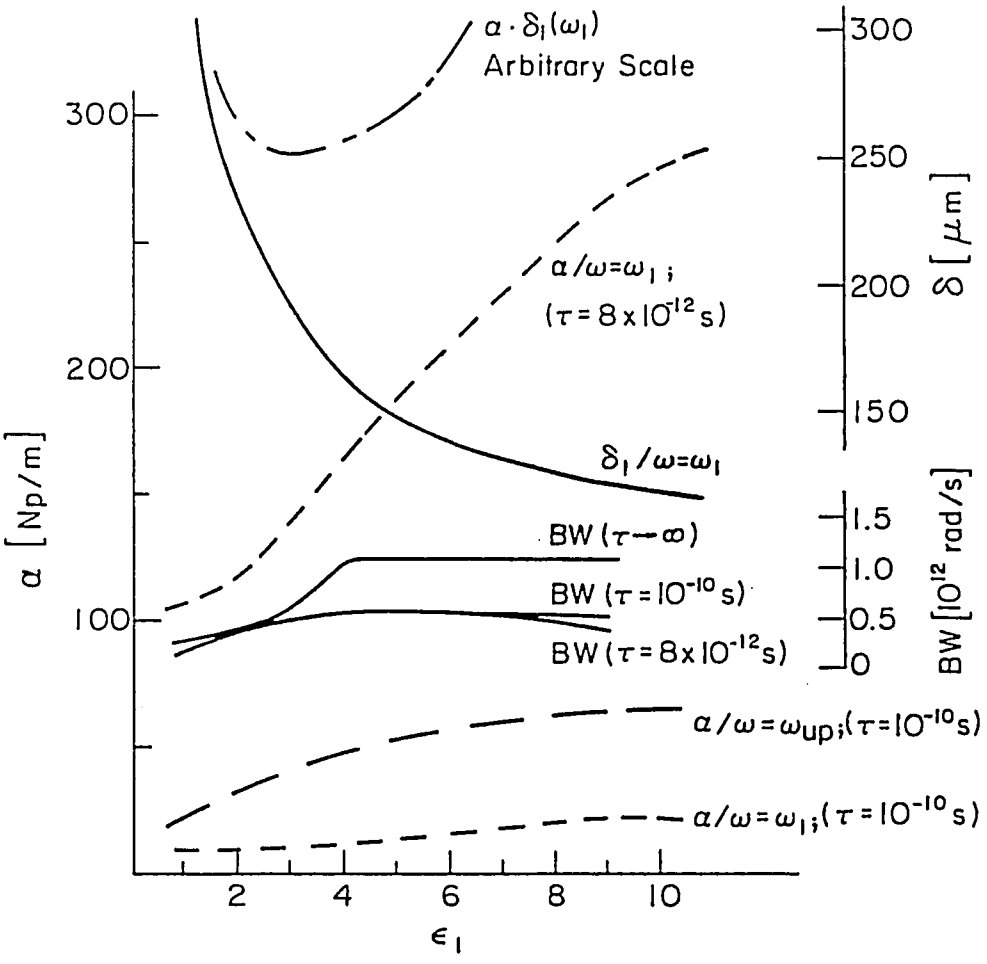

Figure 3 Attenuation constant α, transverse decay factor in dielectric δ_1 (d_1 in the text) and useful bandwidth BW versus dielectric loading ε_1.
$\omega_p = 10^{13}$ rad/s, $\varepsilon^{(0)} = 13$, $\omega_c = 10^{12}$ rad/s.

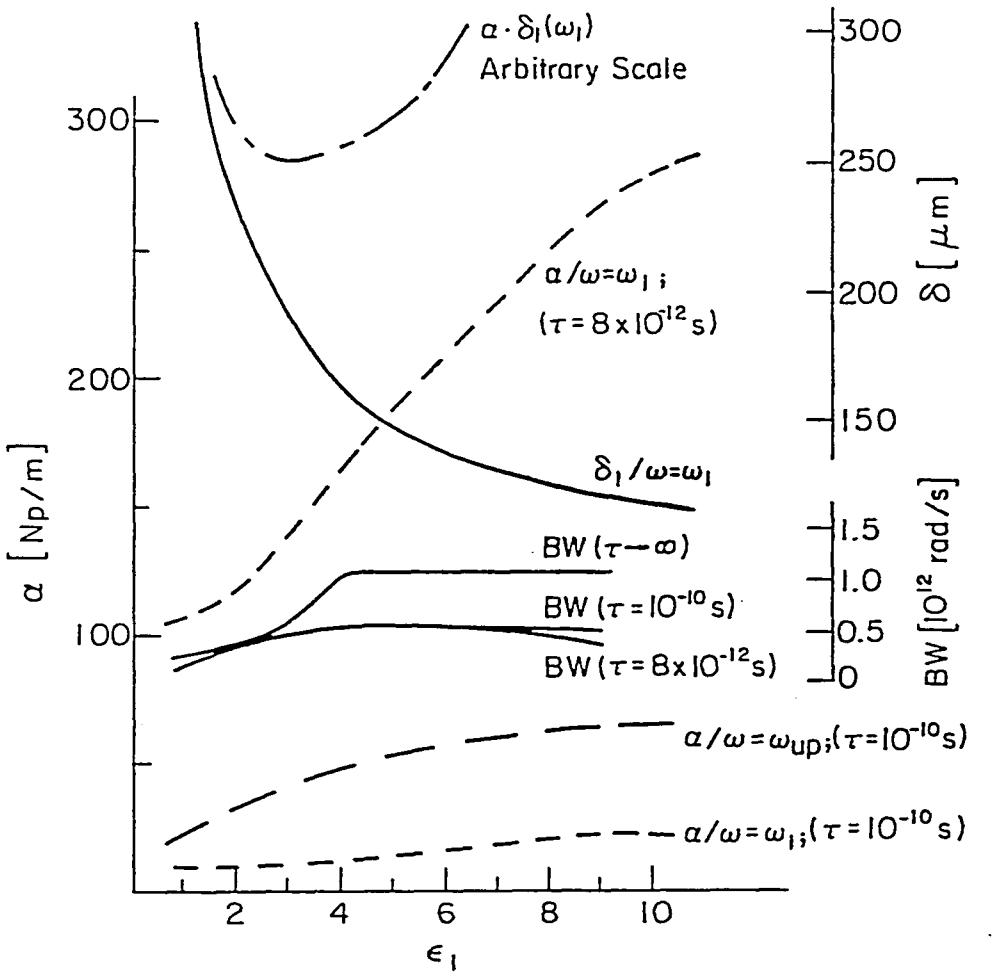

Figure 3 Attenuation constant α, transverse decay factor in dielectric δ_1 (d_1 in the text) and useful bandwidth BW versus dielectric loading ε_1.
$\omega_p=10^{13}$rad/s, $\varepsilon^{(0)}=13$, $\omega_c=10^{12}$rad/s.

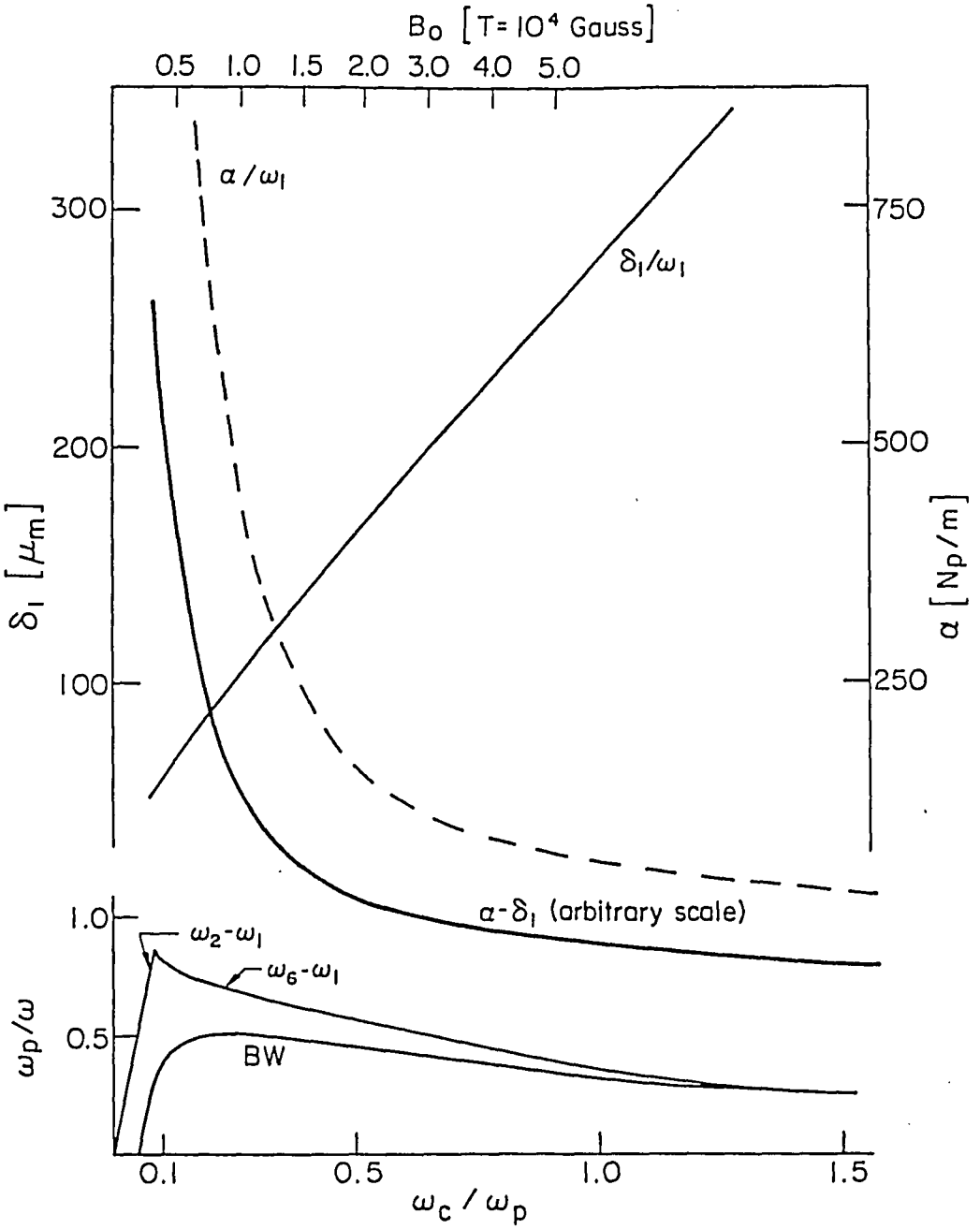

Figure 4 Attenuation constant α, transverse decay factor δ_1 (d_1 in the text) and useful bandwidth BW versus the biasing magnetic field B_o. Other parameters as for Figure 3.

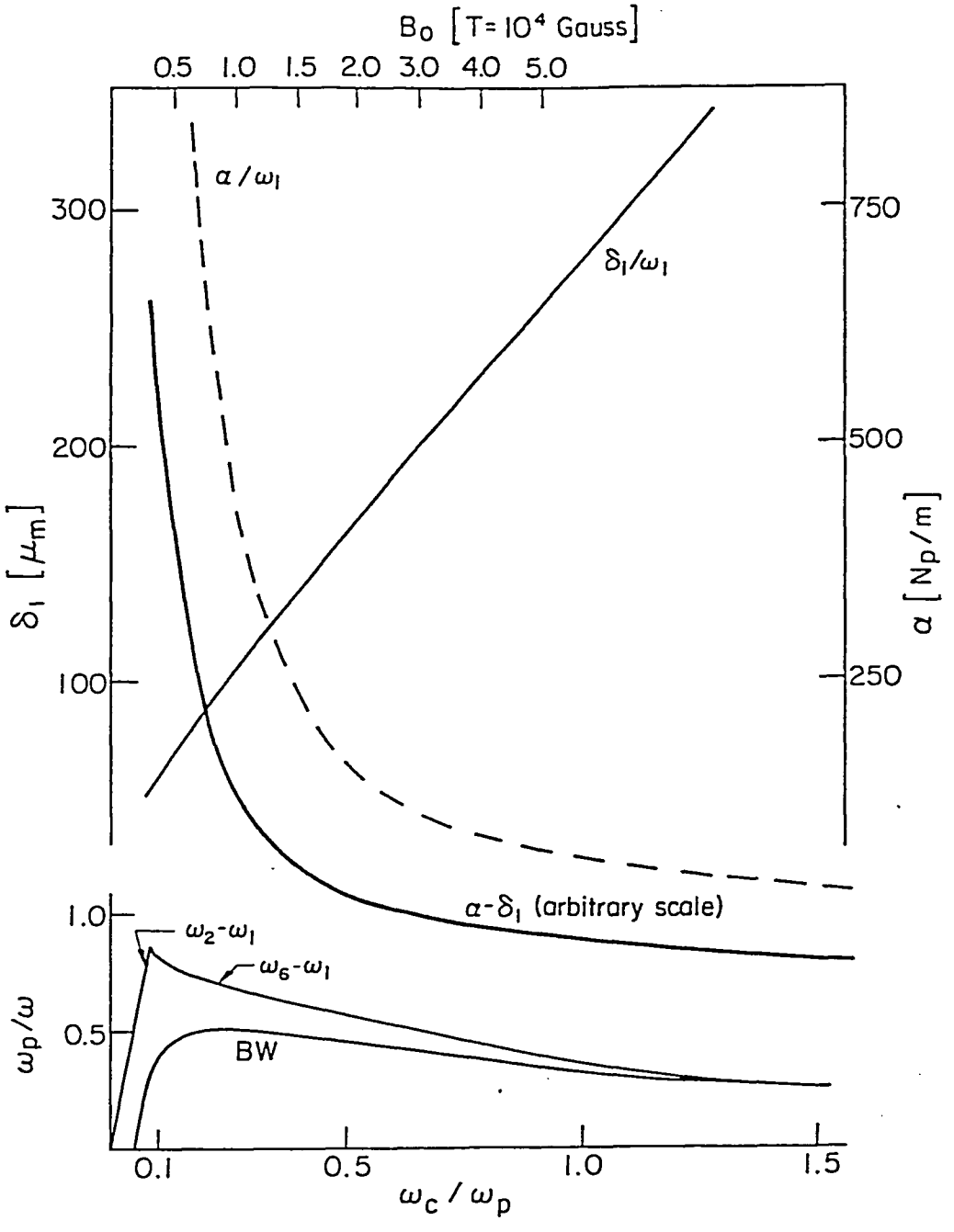

Figure 4 Attenuation constant α, transverse decay factor δ_1 (d_1 in the text) and useful bandwidth BW versus the biasing magnetic field B_o. Other parameters as for Figure 3.

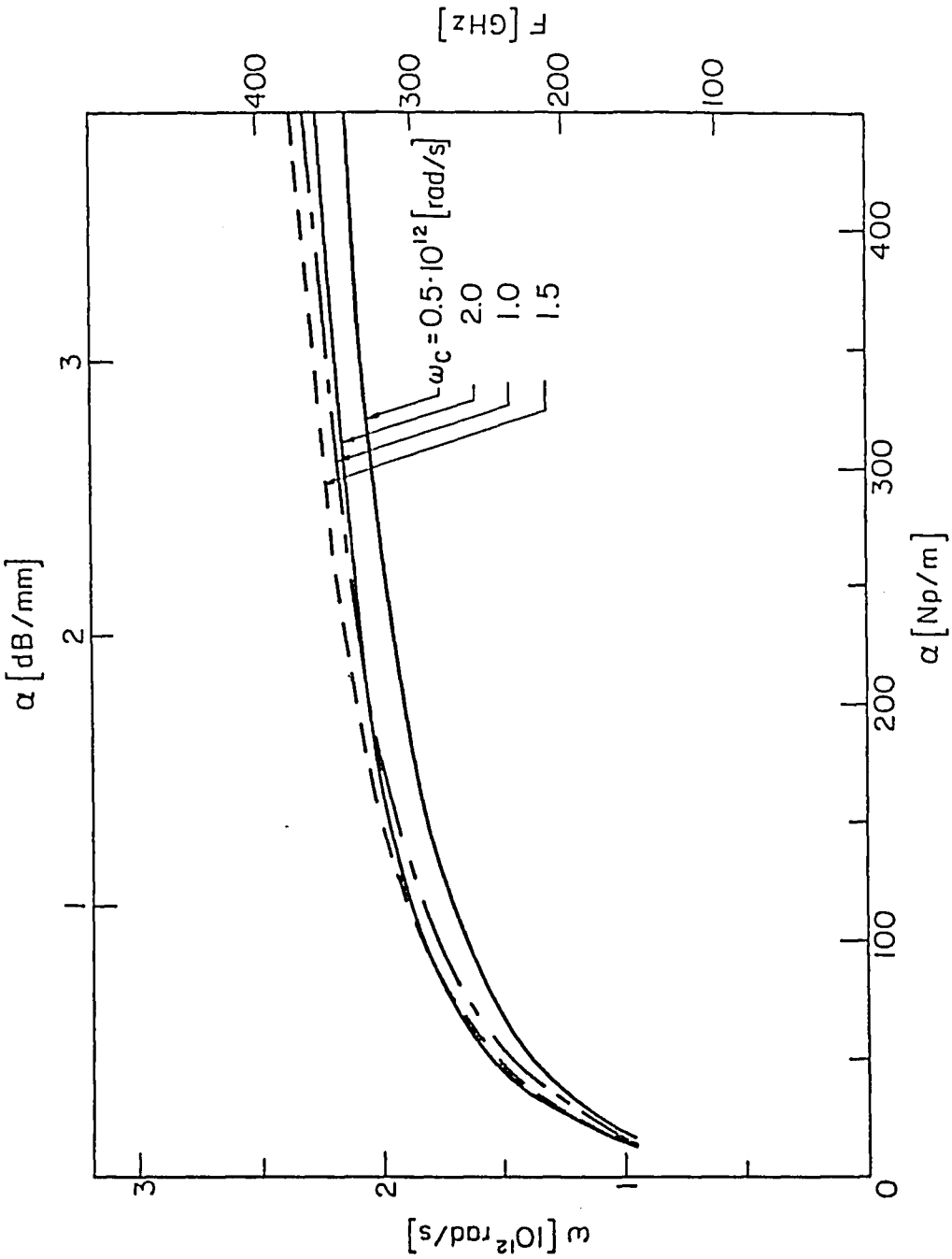

Figure 5 Attenuation constant α versus frequency ω. Parameter ω_c, the cyclotron frequency.

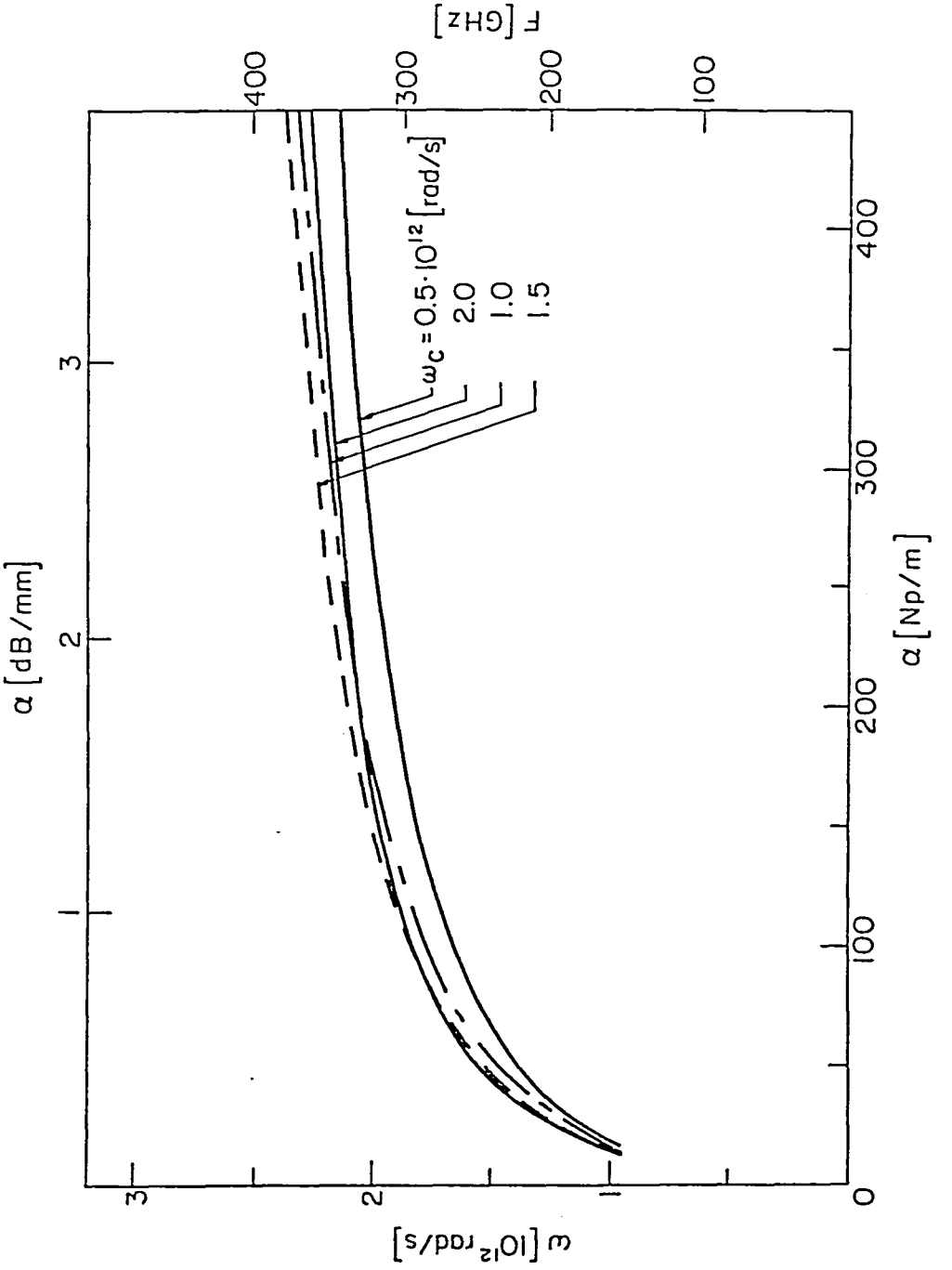

Figure 5 Attenuation constant α versus frequency ω. Parameter ω_c, the cyclotron frequency.

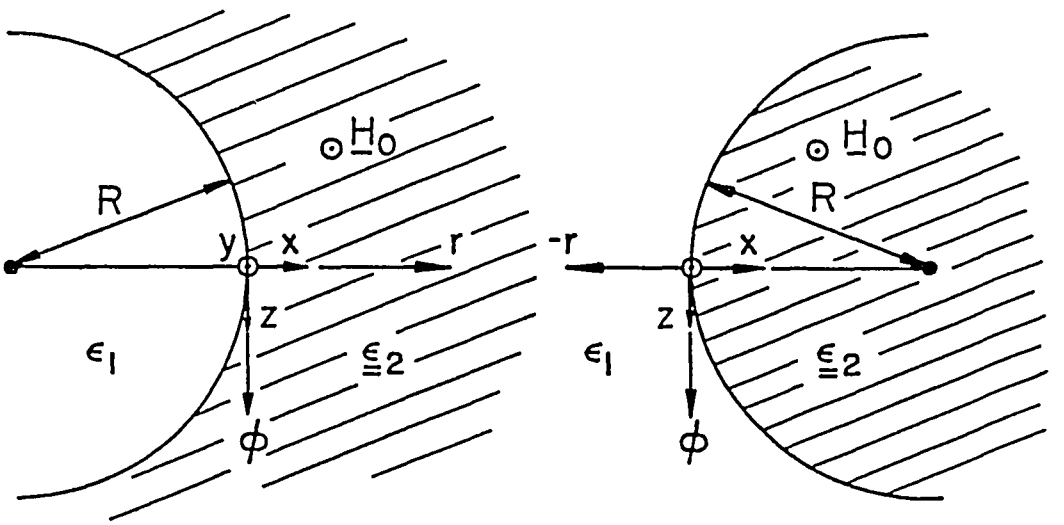

Figure 6.a

Figure 6.b

Figure 6.a Dielectric-semiconductor curved interface.
6.b Semiconductor-dielectric curved interface.

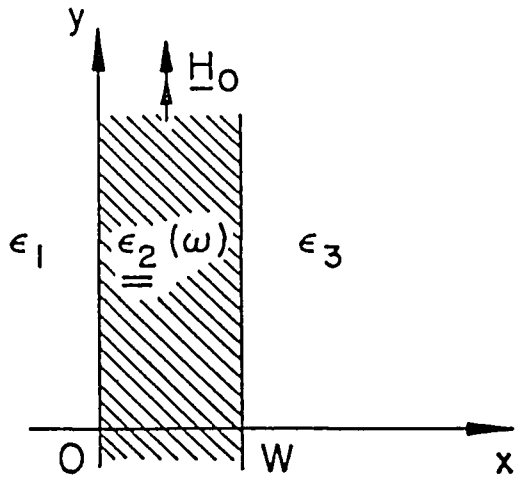

Figure 9.a Single semiconducting slab sided by dielectrics.

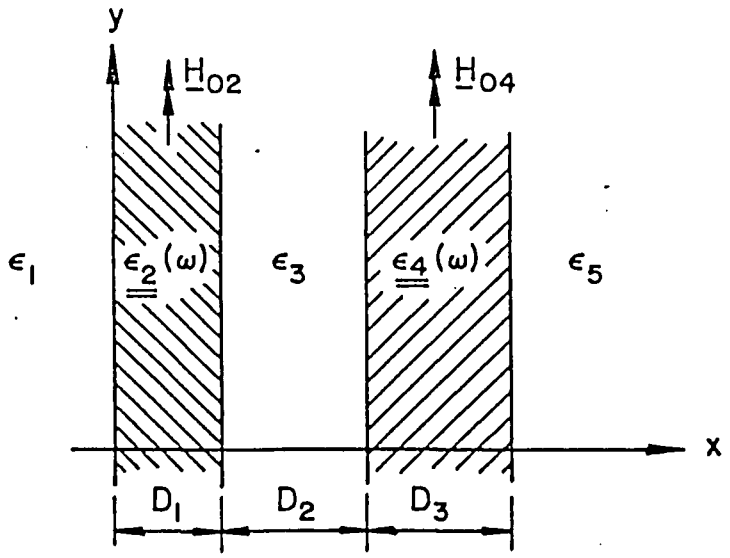

Figure 9.b Five-region canonical structure: double semiconducting slabs sided by dielectrics.

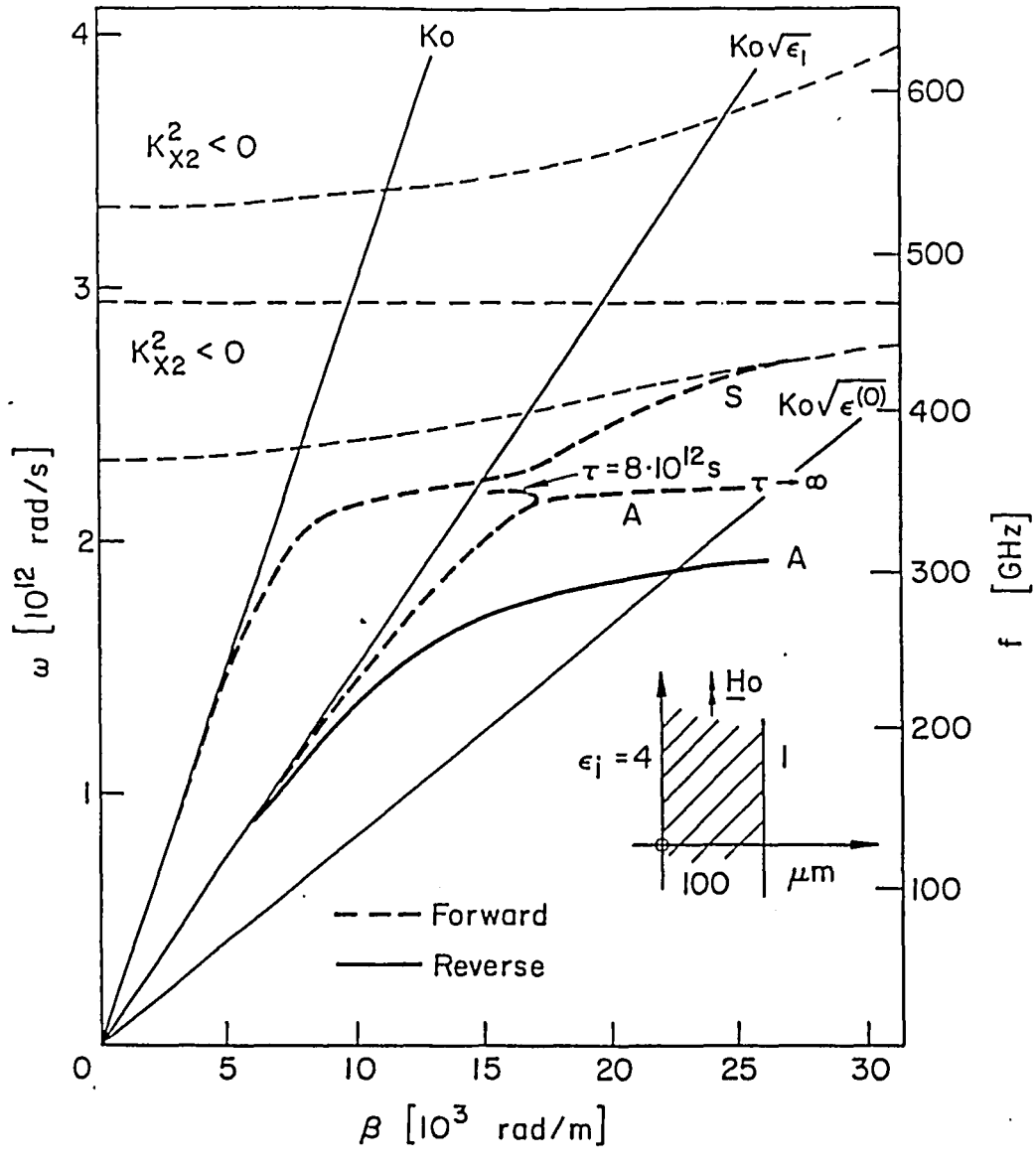

Figure 10.a Sample dispersion diagram for asymmetrically loaded anisotropic n-GaAs slab. Lower modes.
$\omega_p=10^{13}$rad/s, $\varepsilon^{(0)}=13$, $\tau=8\times10^{-12}$s, $\omega_c=10^{12}$

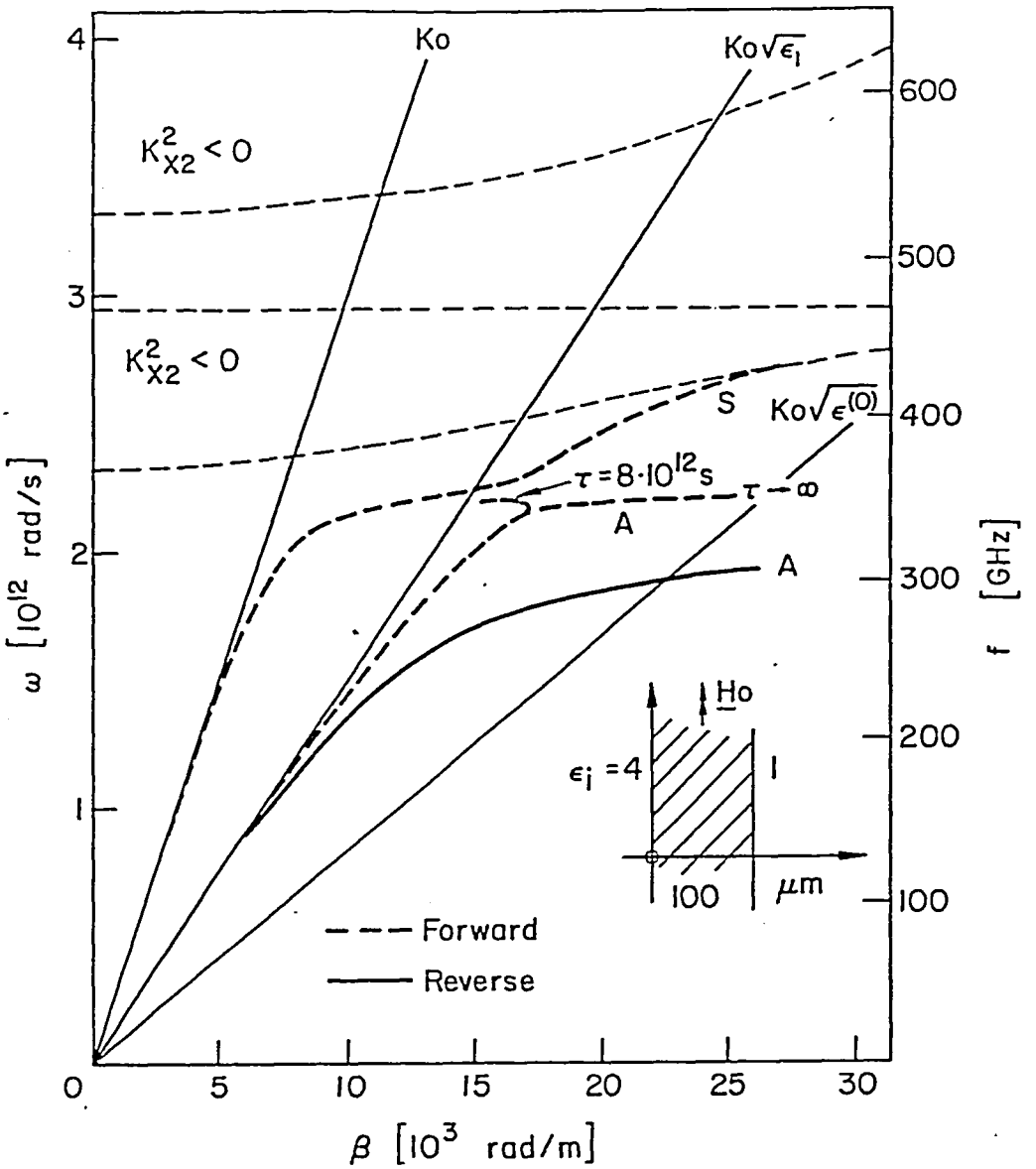

Figure 10.a Sample dispersion diagram for asymmetrically loaded anisotropic n-GaAs slab. Lower modes.
$\omega_p = 10^{13}$ rad/s, $\varepsilon^{(0)} = 13$, $\tau = 8 \times 10^{-12}$ s, $\omega_c = 10^{12}$

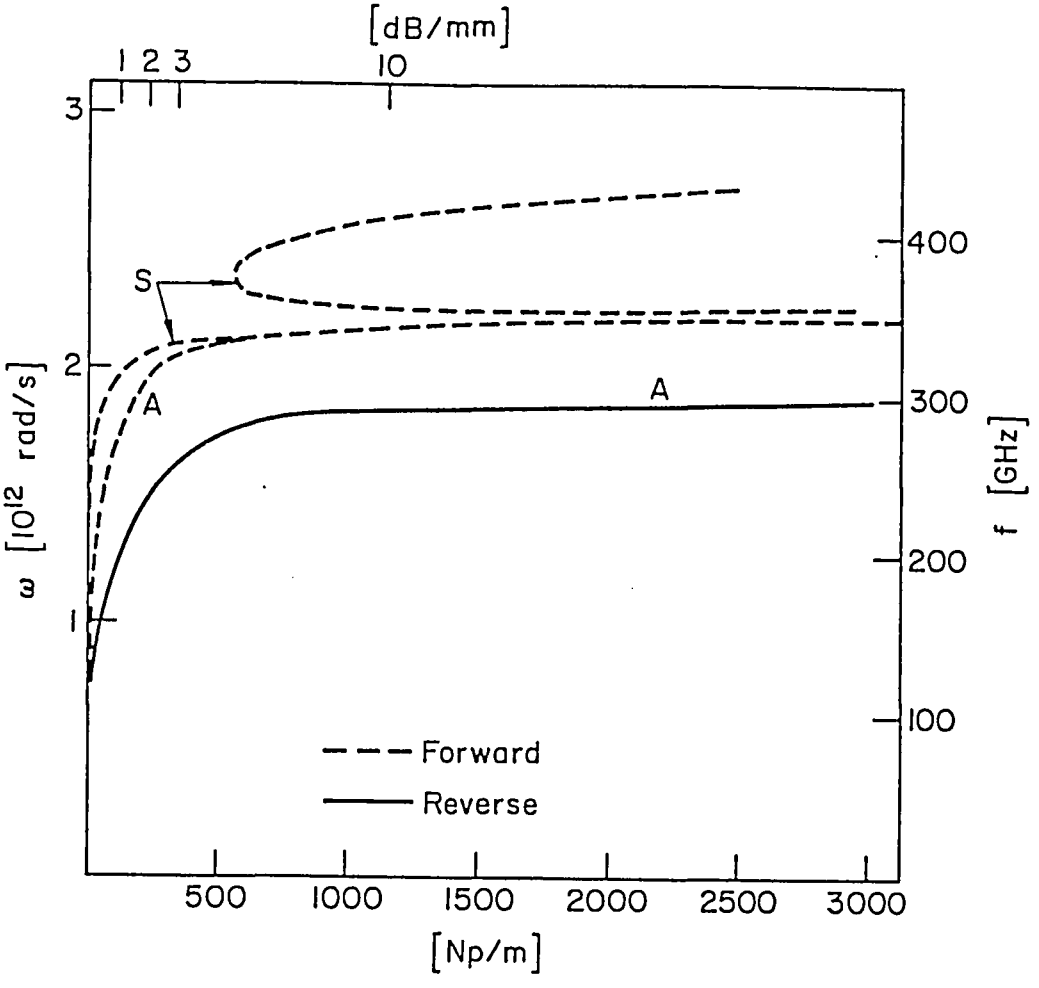

Figure 10.b Attenuation characteristic for the case of Figure 10.a.

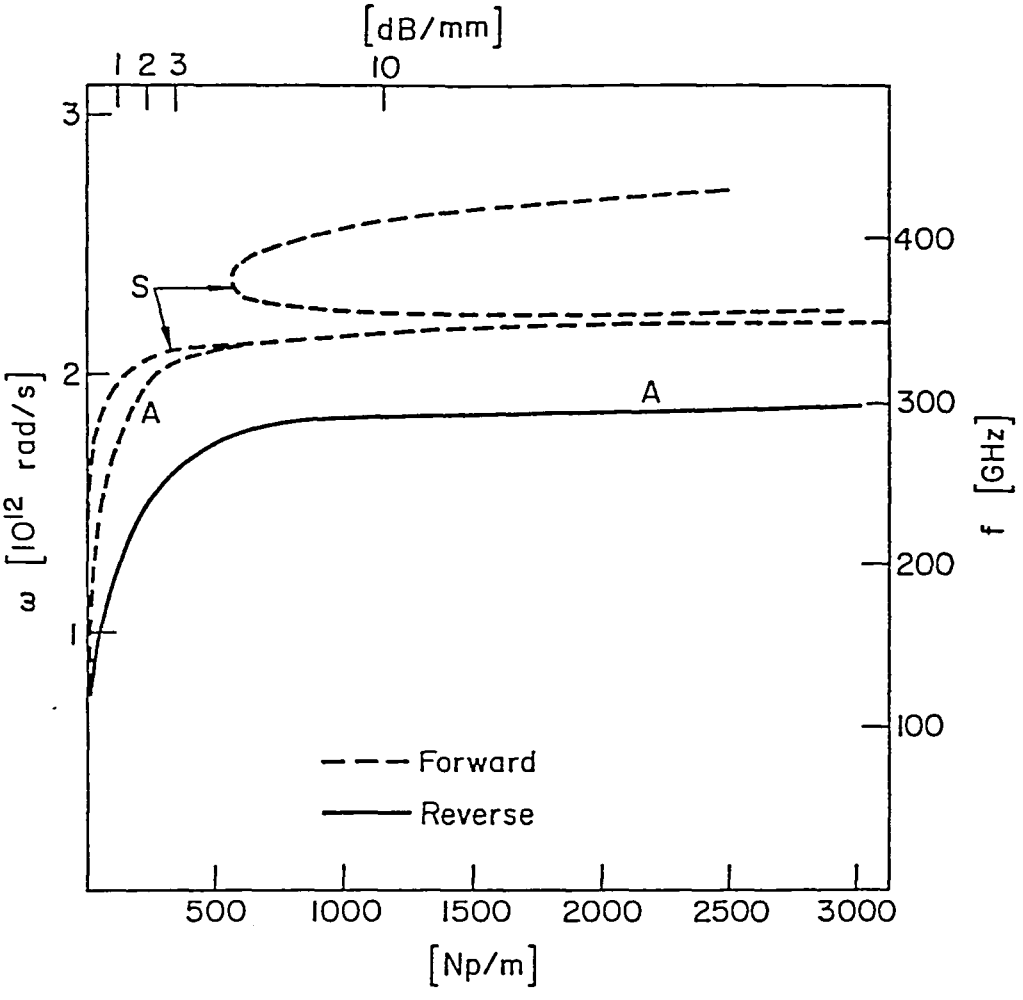

Figure 10.b Attenuation characteristic for the case of Figure 10.a.

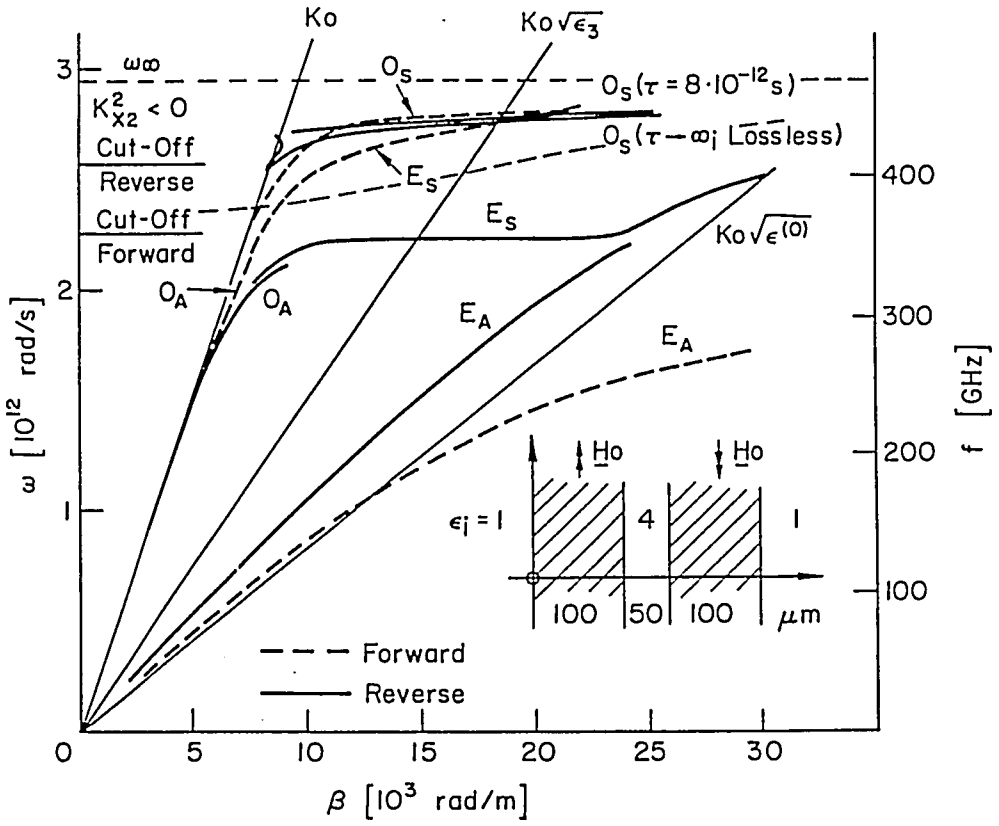

Figure 11.a Dispersion diagram for double n-GaAs slabs. Lower frequency modes.
$\omega_p = 10^{13}$ rad/s, $\varepsilon^{(0)} = 13$, $\tau = 8 \times 10^{-12}$ s,
$\omega_c = 10^{12}$ rad/s.

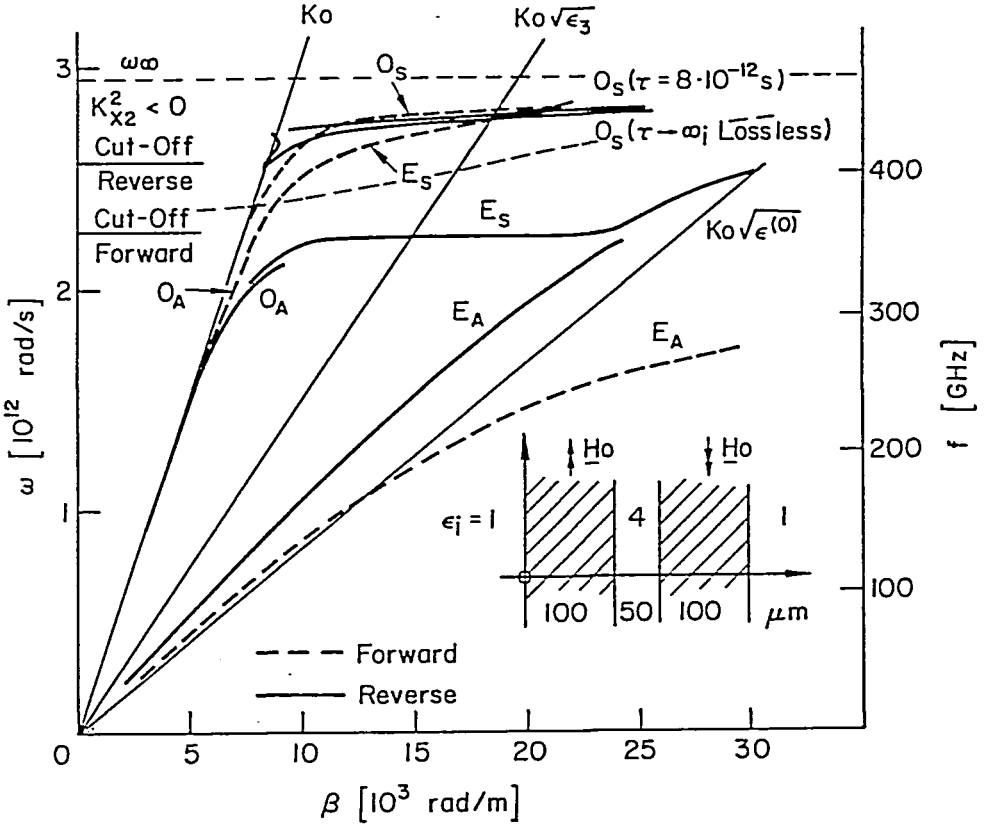

Figure 11.a Dispersion diagram for double n-GaAs slabs. Lower frequency modes.
$\omega_p=10^{13}$rad/s, $\varepsilon^{(0)}=13$, $\tau=8\times10^{-12}$s,
$\omega_c=10^{12}$rad/s.

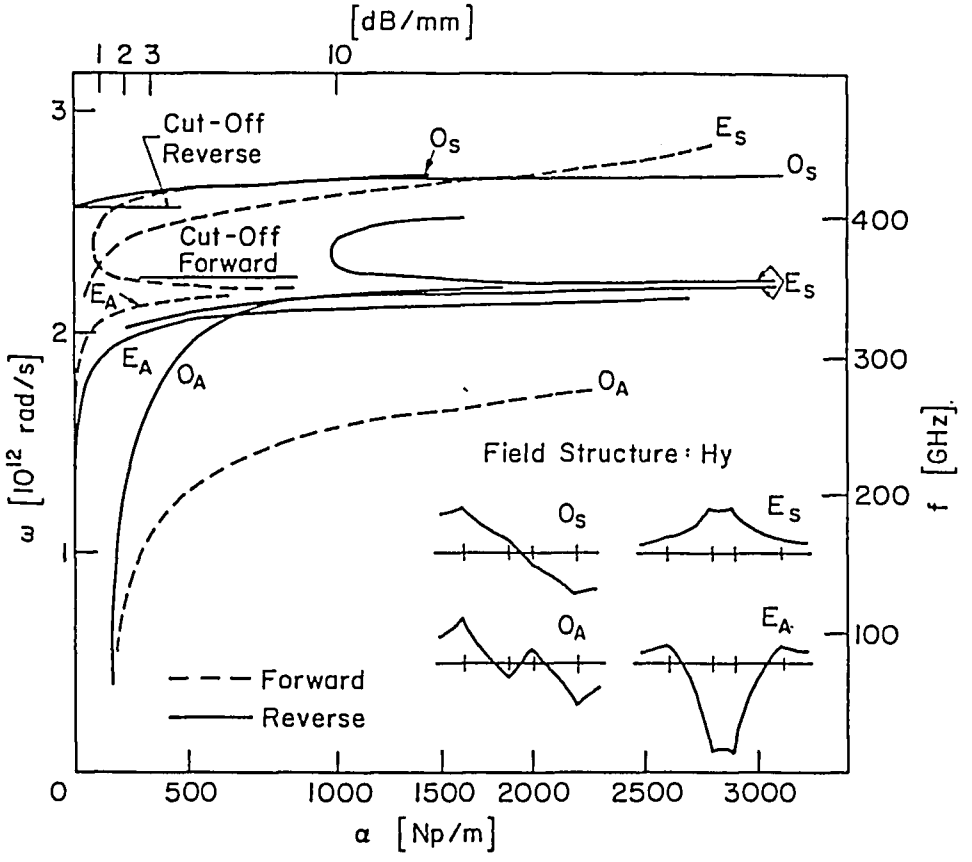

Figure 11.b Attenuation characteristic for the case of Figure 11.a.

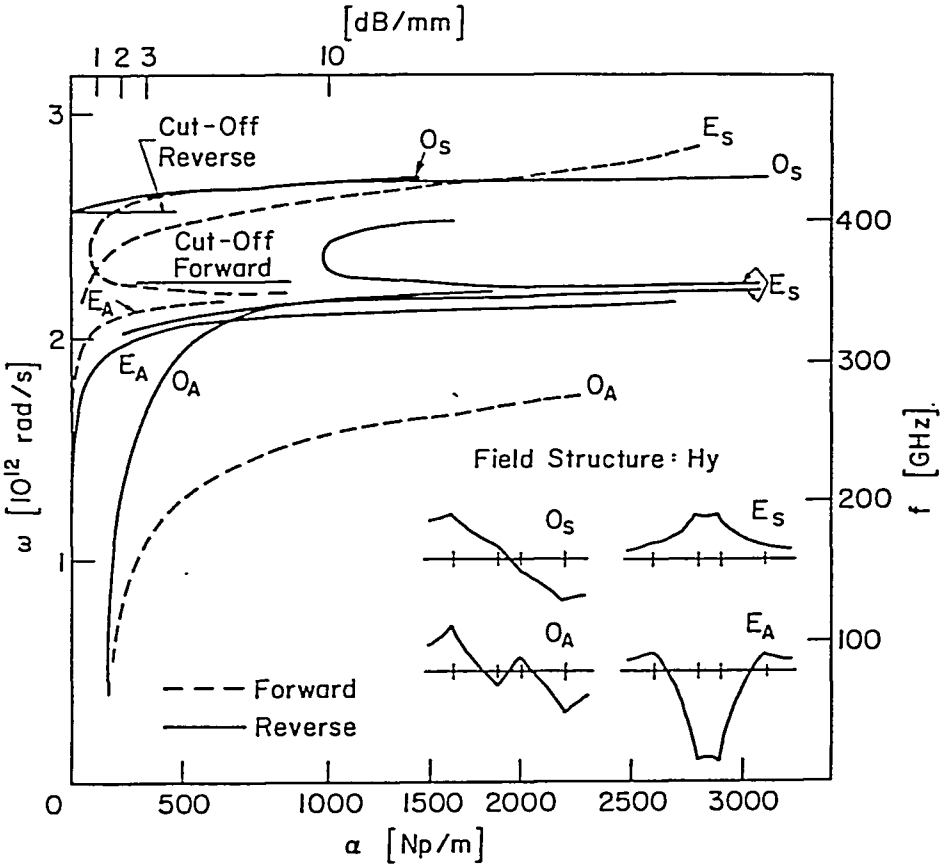

Figure 11.b Attenuation characteristic for the case of Figure 11.a.

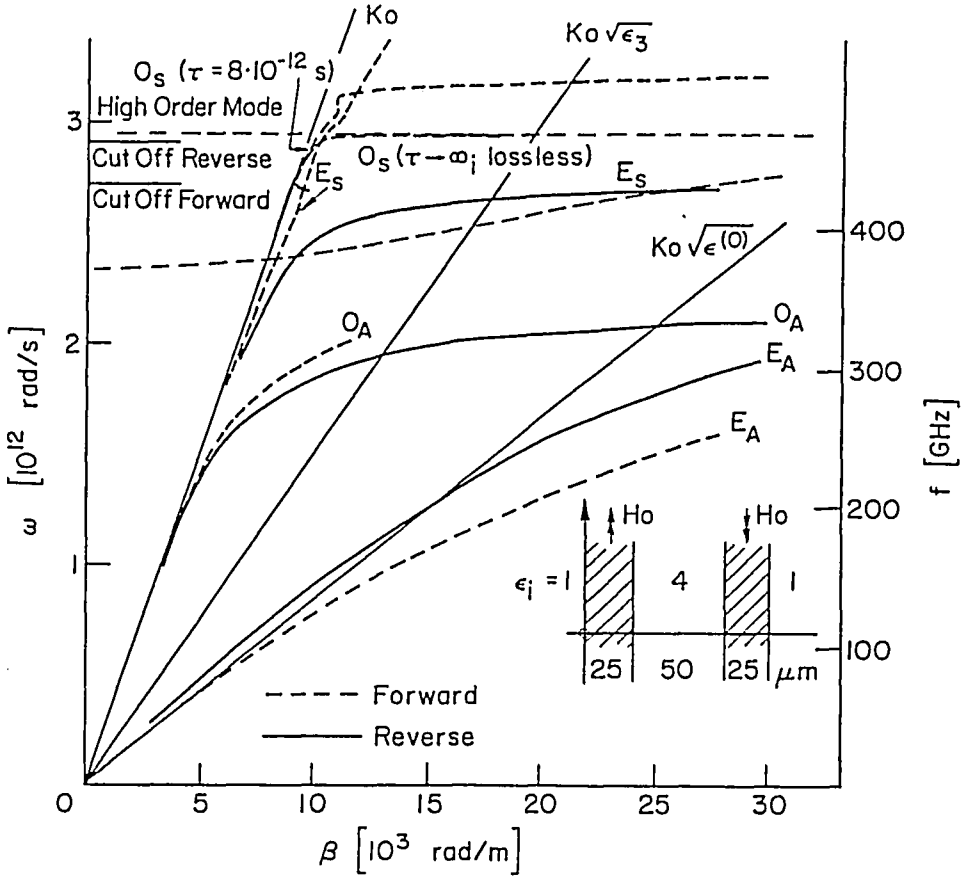

Figure 12.a Same as in Figure 11.a. Other geometry.

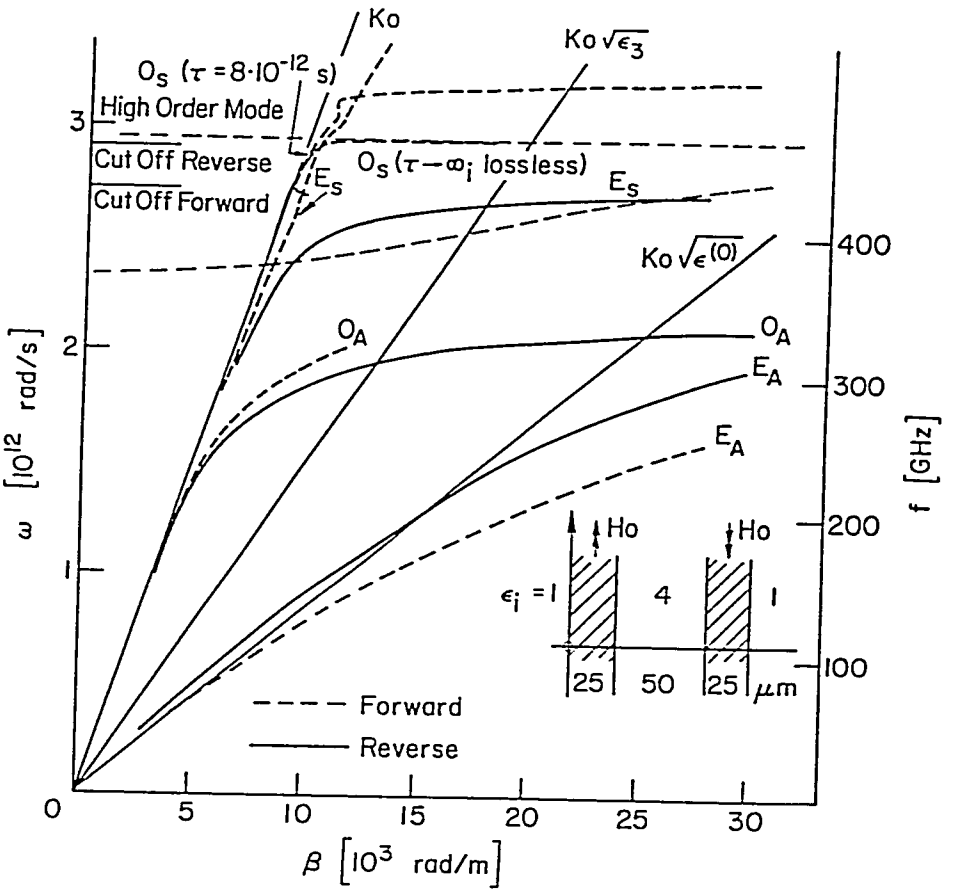

Figure 12.a Same as in Figure 11.a. Other geometry.

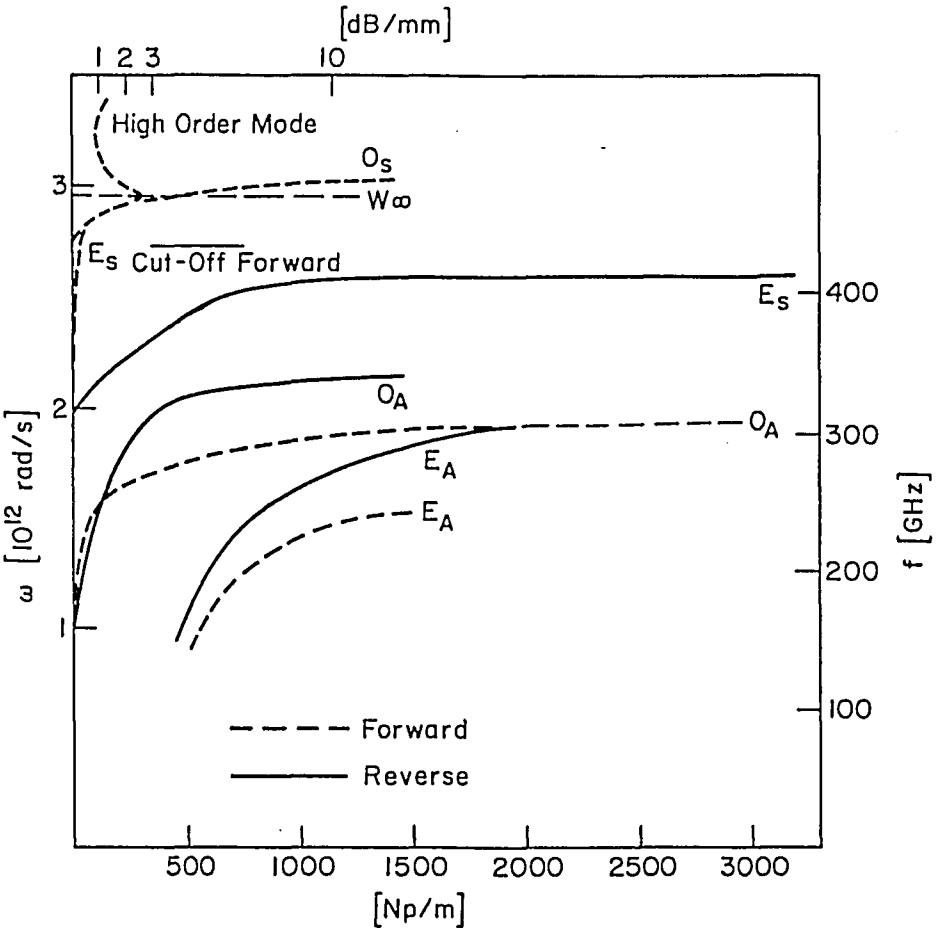

Figure 12.b Attenuation characteristic for the case of Figure 12.a.

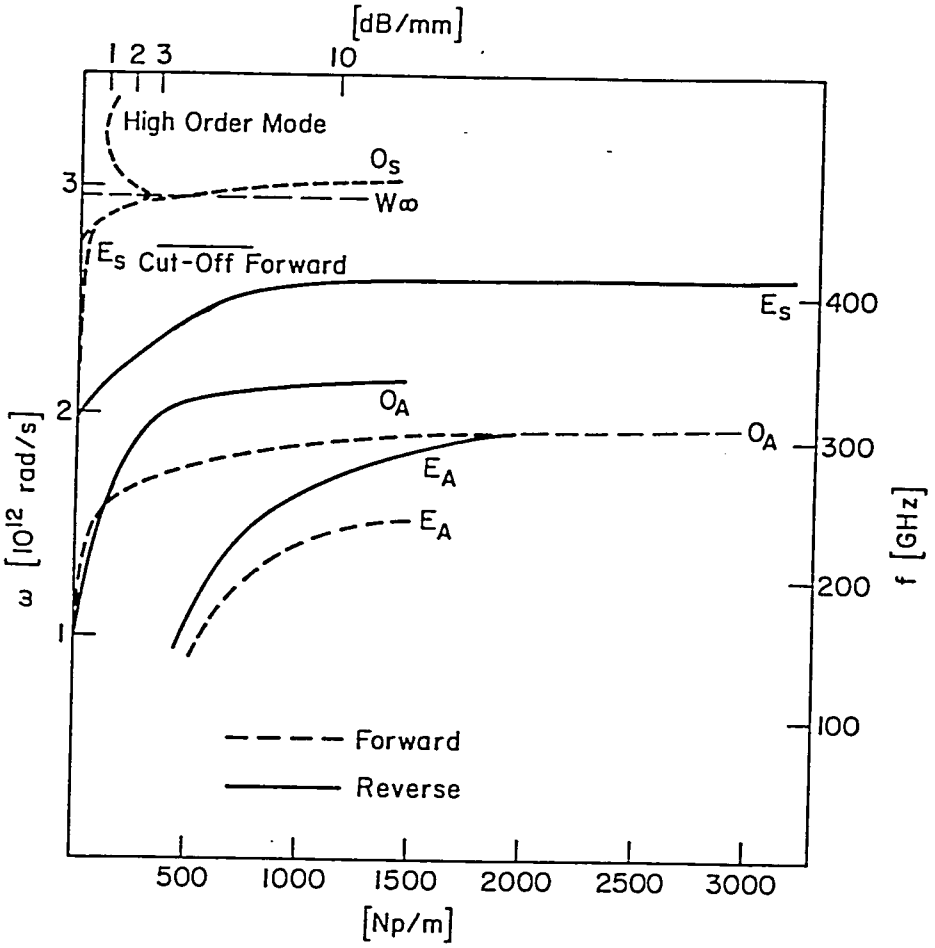

Figure 12.b Attenuation characteristic for the case of Figure 12.a.

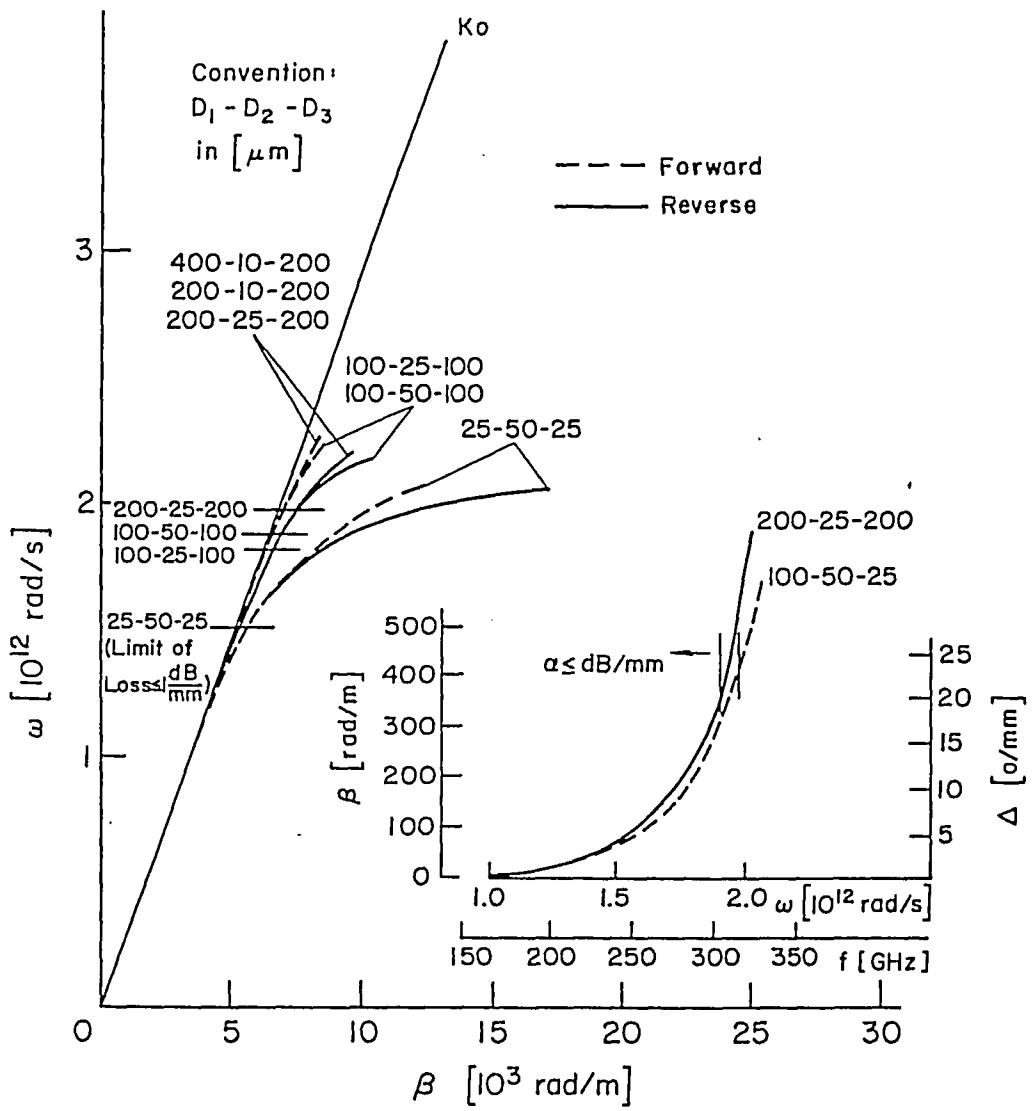

Figure 13 Phase-shift capabilities of O_A modes.

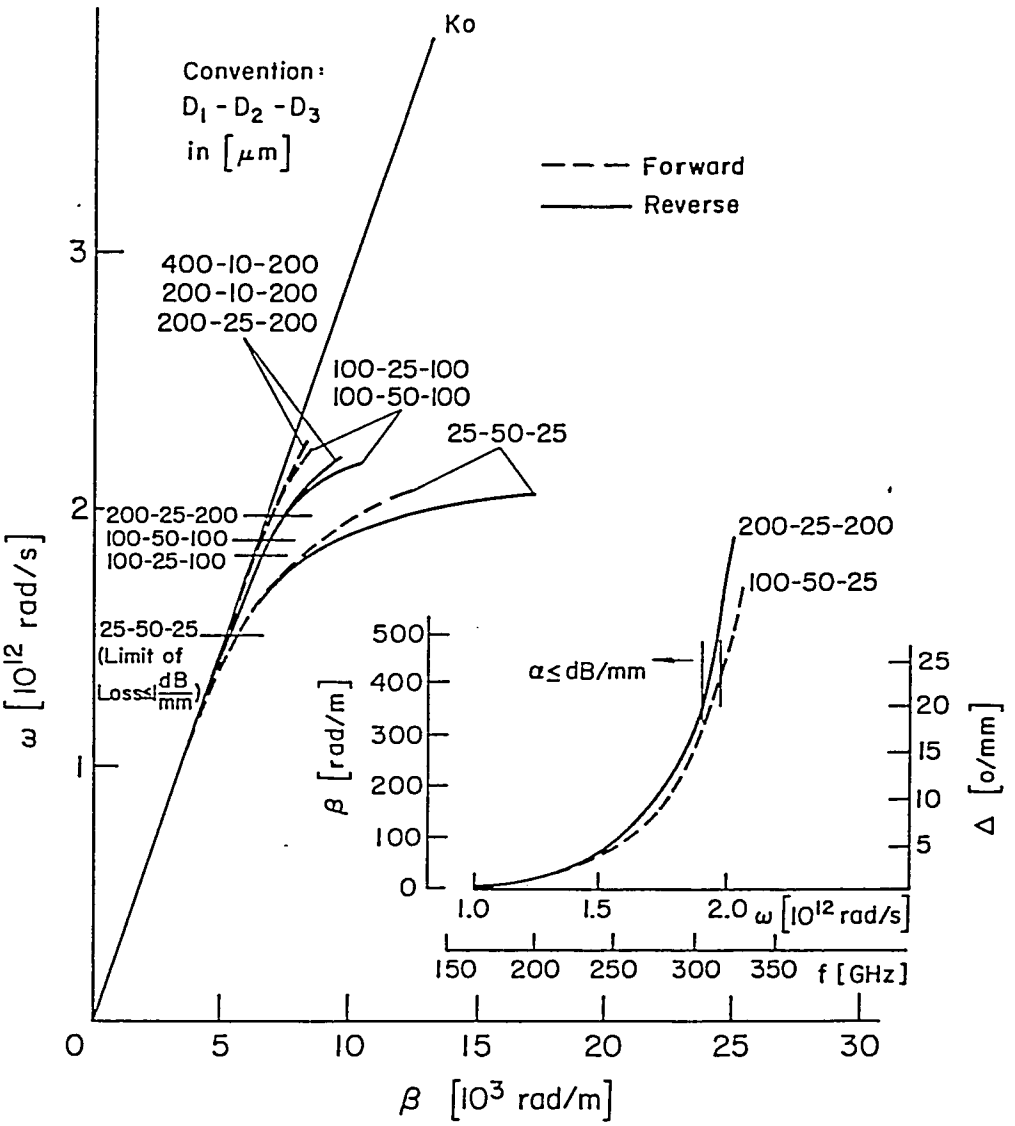

Figure 13 Phase-shift capabilities of O_A modes.

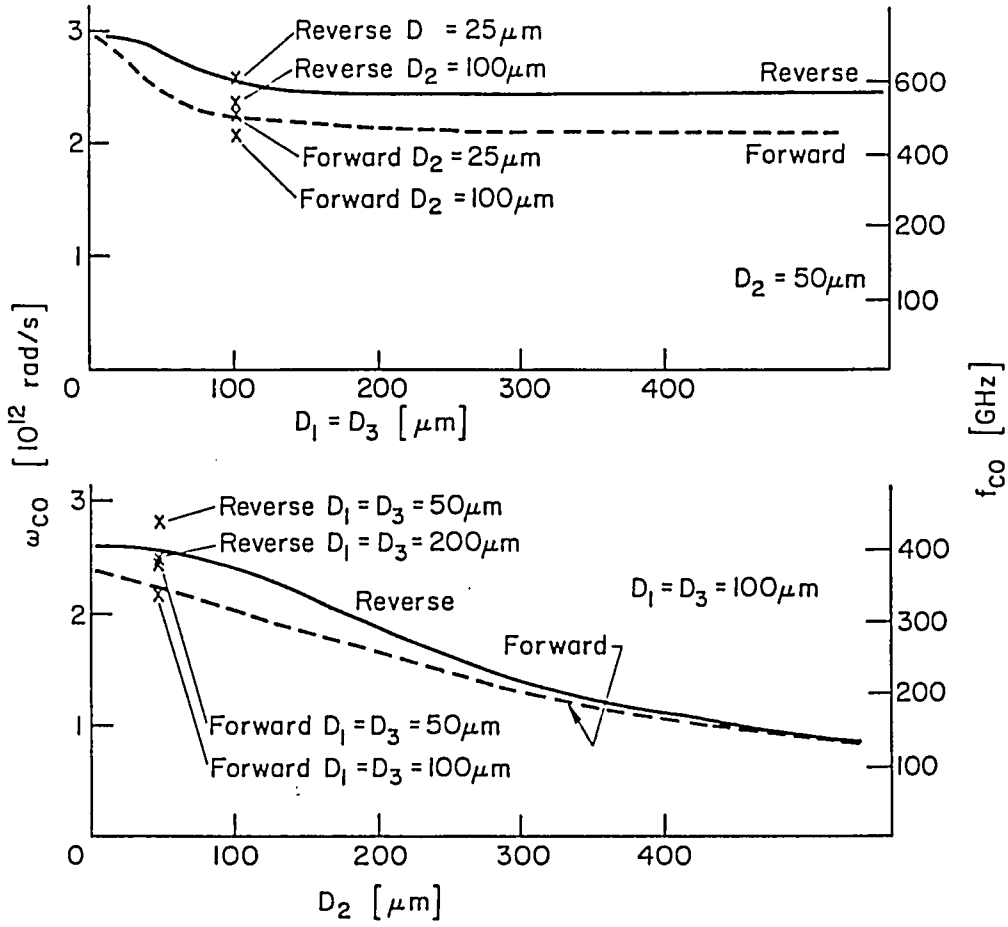

Figure 14 O_S mode cut-off frequency function of the geometry.

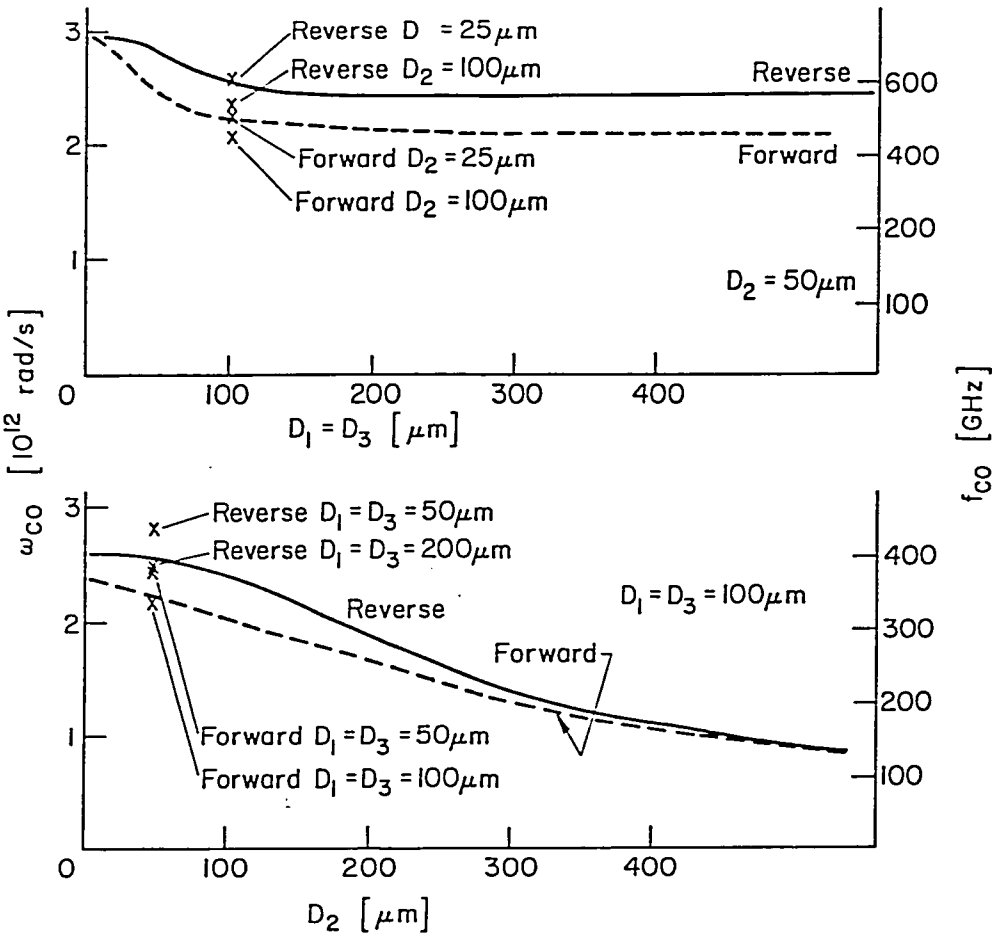

Figure 14 0_S mode cut-off frequency function of the geometry.

REFERENCES

1. D.M. Bolle, S.H. Talisa "Fundamental Considerations in Millimeter and Near-Millimeter Component Design Employing Magnetoplasmons" IEEE-Trans., Mtt-29, Sept. 1981, 961.

2. S.H. Talisa, D.M. Bolle "Preformance Predicions for Isolators and Differential Phase-Shifters for the Near-Millimeter Wave Range" IEEE-Trans., MTT-29, Dec. 1981, 1338.

3. S.H. Talisa, D.M. Bolle "Studies of Nonreciprocal Effects in Planar Near-Millimeter Waveguding Structures" ONR- contract N0014-80-C-0982, Tech. report No.1, May 1981.

4. Whei-lin Hwang, S.H. Talisa, D.M. Bolle "New Results for Near-Millimeter Wave Isolators and Phase-Shifters Based on Magnetoplasmons on GaAs Substrates" Int. J. Infrared and MM Waves, 3, 1982, 253.

5. Whei-Lin Hwang, S.H. Talisa, D.M. Bolle "Studies of Nonreciprocal Effects in Planar Near-Millimeter Waveguding Structures" ONR- contract N0014-80-C-0982, Tech. report No.2, May 1982.

6. M.E. Hines "Reciprocal and Nonreciprocal Modes of Propagation in Ferrite Stripline and Microstrip Devices" IEEE-Trans., MTT-19, May 1971, 442.

7. K.E. Mortenson et al. "A Review of Bulk Semiconductor Microwave Control Components" IEEE-Proc.-59, No 8, Aug. 1971, 1191.

8. A.M. Vaucher, C.D. Striffler, C.H. Lee "Theory of Optically Controled MM Wave Phase Shifters" IEEE-Trans., MTT-31, Feb. 1983, 209.

9. M.G. Li et al. "Wide Bandwidth, High-Repetition-Rate Optoelectronic Modulators of MM Waves in GaAs waveguide" Electron. Lett., Vol. 18, No 11, May 1982, 454.

10. D.M. Marcuse "Bending Losses of the Asymmetric Slab Waveguide" B.S.T.J.-50, No 8, Oct. 1971, 2551.

11. E.A.J. Marcatili "Bends in Optical Dielectric Guides" B.S.T.J.-48, No 7, Sept. 69, 2103.

12. L. Lewin "Radiation from Curved Dielectric Slabs and Fibers" IEEE-Trans., Mtt-22, July 1974, 718.

13. L.M. Ryshik, L.S. Gradstein "Tables of Series, Products and Integrals" VEB, Berlin 1957, p322. (or New York: Academic Press, 1965).

14. G.N. Watson "A Treatise on the Theory of Bessel Functions" 2nd edition, University Press, Cambridge 1944, Chap. 3.

15. A. Erdelyi "Higher Transcendental Functions" McGraw-Hill, New York 1953, p87.

16. COMBES "Bessel Functions for Complex Argument and Order" 11/15/65, AEC Computing and Applied Mathematics Center, New York University, New York, NY 10012.

17. R.E. Collin "Field Theory of Guided Waves" McGraw-Hill, New York 1960, section 11.5.

18. F.W.J. Olver "Asymptotics and Special Functions" Academic Press, 1974, 134.

19. P. de Santis "Edge-Guided Mode in Ferrite Microstrip with Curved Edges" Applied Physics, 4, 1974, 167.

I. APPENDIX

I.1 Asymptotic values

For the radius R tending to infinity we show that the relation obtained for the curved geometry leads to those derived for the plane interface case.

Propagation constant:

For the curved structure we have assumed a propagation factor $\exp[j(\omega t - v\phi)]$. In the flat interface case this factor was $\exp[j\omega t - \gamma z]$. When the radius R tends to infinity the z-axis of the straight coordinates system can be used to describe the curved coordinates system through the relation:

$$z = R\phi \tag{5.1}$$

The two propagation factor are equivalent so that we have:

$$\lim_{R\to\infty} (jv\phi) = \gamma z \tag{5.2}$$

$$\text{hence } \lim_{R\to\infty} (v/R) = -j\gamma \tag{5.3}$$

using (3.6) the relation (3.24) is readily proved.

Dispersion relation:

We prove in the following that the dispersion relation for the curved structure (3.21) leads to the one for the straight geometry (1.15) as the radius R tends to infinity. Comparing these two equations and using the above result (3.24) it only remains to prove

that the equality (3.25) holds.

When the radius R tends to infinity, the transverse coordinate r is best described by the relation:

$$\pm r = R \pm x \qquad (+ \text{ Fig.6.a; } - \text{ Fig.6.b}) \tag{5.4}$$

which shows the dependance of the r-coordinate on the radius R. The x-coordinate corresponds directly to the x-axis of the straight waveguide.

In the case of large radii, both the order and argument of the Bessel functions considered are large. Therefore, the following approximations may be used [13-14]:

for $u_i = k_o\sqrt{\epsilon_i}\,r$ or $k_o n r$ if $\epsilon_e' > 0$

ch $t = v/u_i$

$$J_v(u_i) \sim \sqrt{\frac{1}{2\pi v \tanh t}}\, \exp[\, v \tanh t - vt \,] \tag{5.5}$$

$$H_v^{(2)}(u_i) \sim -j\sqrt{\frac{2}{v\pi \tanh t}}\, \exp[-v \tanh t + vt] \tag{5.6}$$

for $u_i = j\, k_o n r$ if $\epsilon_e' < 0$

sh $t = v/u_i$

$$J_v(u_i) \sim \sqrt{\frac{1}{2\pi v \coth t}}\, \exp\{[\, v \coth t - vt] + jv\pi/2\} \tag{5.7}$$

$$H_v^{(2)}(u_i) \sim \sqrt{\frac{2}{v\pi \coth t}}\ \exp\{[-v \coth t + vt] + jv\pi/2\} \tag{5.8}$$

Thus, using the relation

$$\operatorname{arctanh} z = .5 \ln[(1+z)/(1-z)] \qquad ; z^2 < 1$$

$$F_v(u_i) \sim \sqrt{\frac{1}{K}}\ \exp \pm\{v - \frac{1}{2} \ln(\operatorname{abs}[\frac{1+K/v}{1-K/v}]) - K\} \tag{5.9}$$

$$\text{where}\quad K^2 = v^2 - u_2 = v^2 - k_o^2 \epsilon_i r^2 \qquad i=1,2\ (\epsilon_2 = \epsilon_e) \tag{5.10}$$

The minus sign is chosen if $F_v(u_i)$ represents the Bessel function of the first kind and the positive sign stands for the case where the Hankel function is used.

Let us consider the case where positive signs are used in both relation (5.4) and (5.9). Other cases will be readily derived from the following analysis developed by Marcuse [10] which is repeated here for the reader's convenience.

For large radius R, (5.4) is rewritten as:

$$r/R = 1 + x/R \qquad \text{where} \quad x/R << 1$$

Thus, the expression (5.10) becomes:

$$K^2 = v^2 - k_o^2 \epsilon_i R^2 (1+x/R)^2$$

$$K^2 = v^2 - k_o^2 \epsilon_i R^2 (1+2x/R)$$

hence

$$K = k_i R\ (1 - k_o^2 \epsilon_i / k_i^2\ x/R) \tag{5.11}$$

where

$$k_i^2 R^2 = v^2 - k_o^2 \epsilon_i$$

or using (3.6):

$$k_i^2 = \beta_v^2 - k_o^2 \epsilon_i \qquad i=1,2 \quad (\epsilon_2 = \epsilon_e) \tag{5.12}$$

Note that k_i correspond exactly to the transverse exponential factors used in the flat interface case. Indeed for R approaching infinity, the use of (3.24) gives:

$$k_i^2 = -\gamma^2 - k_o^2 \epsilon_i$$

In the denominator of the expression (5.9), we can use the approximation:

$$\sqrt{K} \cong \sqrt{k_i R} \tag{5.13}$$

However the expression in the exponent must be approximated more accurately. Let us first derived the following result:

if $a=b(1+d)$ with $a<1$ and $d<<1$ then $a^n=b^n(1+nd)$
and
$1/2\ \ln[(1+a)/(1-a)] = \text{arc th } a = a+a^3/3+a^5/5+\ldots=$

$=b+b^3/3+b^5+\ldots+bd(1+(b^2)+(b^2)^2+\ldots)=$

$=1/2\ \ln[(1+b)/(1-b)] + bd\ /\ (1-b^2)$

In our case $b=k_i/\beta_v$ and $d=k_o^2\epsilon_i/k_i^2 \cdot x/R$

hence, using (5.11) and (5.12) in the exponent of (5.9) and (5.13) in the denominator, the general expression (5.9) for the Bessel function considered becomes:

$$F_v(u_i) \sim (k_i R)^{-1/2} \exp[\ 1/2 \cdot U_i \cdot R - k_i x\ ] \tag{5.14}$$

$$\text{with } U_i = \beta_v \ln\{\text{abs}[\ \frac{1+k_i/\beta_v}{1-k_i/\beta_v}\ ]\} - 2k_i \qquad i=1,2 \tag{5.15}$$

Therefore the transverse magnetic field has the following expression:

in the dielectric region of Figure 6.a: (5.16)

$$H_y = \frac{C}{\sqrt{k_1 R}}\, e^{-.5U_1 R}\, e^{k_1 x}$$

in the dielectric region of Figure 6.b:

$$H_y = \frac{C}{\sqrt{k_1 R}}\, e^{+.5U_1 R}\, e^{k_1 x}$$

in the semiconductor region of Figure 6.a:

$$H_y = \frac{C}{\sqrt{k_2 R}}\, e^{+.5U_2 R}\, e^{-k_2 x}$$

in the semiconductor region of Figure 6.b:

$$H_y = \frac{C}{\sqrt{k_2 R}}\, e^{-.5U_2 R}\, e^{-k_2 x}$$

The derivative of the Bessel functions becomes, with the help of the expression for u_i (3.15),(3.16) and the relation dr=dx from (5.4):

$$F_v'(u_i)=1/(k_o\sqrt{\epsilon_i})\ dF_v(u_i)/dx \tag{5.17}$$

Therefore, the following relations are derived which establishes the equivalence of the dispersion relations for the flat and curved structure as the radius of curvature tends to infinity.

$$\begin{aligned} [u_1/R\ F_v'(u_1)/F_v(u_1)\ ] &= k_1 \\ [u_2/R\ F_v'(u_2)/F_v(u_2)\ ] &= -k_2 \end{aligned} \tag{5.18}$$

It is to be pointed out that the relations derived in this Appendix are valid for R>>x and R large, i.e., in the vicinity of the interface when large radii are considered or for the case of infinite radii R.

I.2 Power

The power carried by the mode is calculated by integrating over the transverse coordinate the component of the Poynting vector which is colinear with the direction of propagation.

$$\begin{aligned} P &= \int_0^\infty S_\phi \, dr \qquad \text{for the curved interface} \\ P &= \int_{-\infty}^{\infty} S_z \, dx \qquad \text{for the plane interface} \end{aligned} \tag{5.19}$$

The computation of S_0 involves Bessel functions which do not allow the power P to be related to the field amplitude (e.g. B) in a simple closed form. Fortunately the expression of S_z is far easier. Thus the power P and field amplitude A for the flat interface case are initially related. Then, a relation between A and B is derived with the help of (5.16) and (1.5). Such a relation is valid only for large radius R as is suggested in the section 3.4.

The power P carried by a mode in the flat interface case is given by:

$$P = \int_{-\infty}^{0} S_{1z} \, dx + \int_0^\infty S_{2z} \, dx$$

where $S_{iz} = \mathrm{Re}[\ 1/2\ E_{xi}H^{*}_{yi}\ ]$ $\quad i=1,2$

From the analysis of the plane geometry ([2],Chap.1), it is readily found:

$$P = \frac{A^2}{4\omega\epsilon_o}\ \mathrm{Re}\left[\frac{\beta}{\epsilon_1}\ \frac{1}{\mathrm{Re}[k_1]} + \left(\frac{\beta}{\epsilon_e} - \frac{\eta k_2}{\xi\epsilon_e} - j\frac{\alpha}{\epsilon_e}\right)\frac{1}{\mathrm{Re}[k_2]}\right] e^{-2\alpha z} \qquad (5.20)$$

In the lossless case, the above expression becomes:

$$p = \frac{A^2}{4\omega\epsilon_o}\left(\frac{\beta}{\epsilon_1 k_1} + \frac{\beta}{\epsilon_e k_2} - \frac{\eta}{\xi\epsilon_e}\right)$$

Now, a relation between A and B is derived in the case of the Figure 6.a (C replaces B in the case of the Figure 6.b). For this purpose the radius R is assumed to be large so that the field in the vicinity of the curved interface can be approximated by the field of the straight structure. Since we are interested in the bending loss due to radiation, we relate the outward field distribution of the curved interface to its correspondent on the plane interface, i.e., we relate A to B in the case of Figure 6.a and A to C in the case of Figure 6.b. In the following, only the first case (Fig.6.a) is derived. The second case (Fig.6.b) is then readily obtained by substituting C for B and 1 for 2. So, in the vicinity of the interface and for large radius R, the field distributions in the curved (5.16) and plane (1.5) structure may be equated, giving:

$$A\ \exp[-k_2 x] = -j\ \ B/\sqrt{k_2 R}\ \ \exp[1/2\ U_2 R]\ \exp[-k_2 x]$$

Therefore the power carried by the mode can be written as:

$$P = \frac{B^2}{4\omega\epsilon_0} \mathrm{Re}[\ldots] \frac{1}{|k_2| R} \exp\{\mathrm{Re}[U_2]\cdot R\} \quad \exp\{-2\alpha z\} \tag{5.21}$$

where $|\ |$ indicates that the magnitude has to be taken and Re[...] refers to the term in (5.20).

I.3 Radiated power

In the curved interface case, the transverse (r-component) of the Poynting vector may be expressed as:

$$S_r = \mathrm{Re}[-1/2\ E_\phi\ H_y^*] = 1/2\ \mathrm{Re}[-E_\phi/H_y]\ \ H_y{}^2$$

$$S_r = 1/2\ Z_r\ |H_y|^2 \tag{5.22}$$

Using the approximation (5.6) and (5.8) for the Hankel function, the transverse magnetic field can be written as follow:

for Figure 6.a

$$H_{y2} = \frac{B}{\sqrt{K}} \exp[\ v\ \mathrm{arctanh}\frac{K}{v} - K\ ] \qquad \text{if } \epsilon_e'>0 \tag{5.23}$$

$$H_{y2} = \frac{B}{\sqrt{K}} \exp[\ v\ \mathrm{arccth}\frac{K}{v} - K\ ] \qquad \text{if } \epsilon_e'<0 \tag{5.24}$$

$$\text{with}\quad K^2 = v^2 - K_0^2\ {}_e r^2 \tag{5.25}$$

for Figure 6.b,

$$H_{y1} = \frac{C}{\sqrt{K}} \exp[\ v\ \mathrm{arctanh}\frac{K}{v} - K\ ] \tag{5.26}$$

$$\text{with}\quad K^2 = v^2 - K_1^2 \epsilon_1 r^2 \tag{5.27}$$

The electric field in the direction of propagation is found with the

help of (3.10) and (3.13):

for Figure 6.a, for all ϵ_e:

$$E_{\phi 2} = \frac{1}{j\omega\epsilon_o\epsilon_e}\left[\frac{k_o^2\epsilon_e r}{K}\left(-\frac{1}{2K}+\frac{v^2}{k_o^2\epsilon_e r^2}-1\right)+\frac{\eta v}{\xi r}\right] H_{y2} \qquad (5.28)$$

and for Figure 6.b:

$$E_{\phi 1} = \frac{1}{j\omega\epsilon_o\epsilon_1}\left[\frac{k_o^2\epsilon_1 r}{K}\left(-\frac{1}{2K}+\frac{v^2}{k_o^2\epsilon_1 r^2}-1\right)\right] H_{y1} \qquad (5.29)$$

Note that the propagation factor $\exp[j(\omega t - v\phi)]$ is impicit in these previous expressions of the electromagnetic fields.

We are interested in the fields expression very far away from the interface, where radiation due to curvature is readily identified. Therefore, we allow r to tend to infinity in the expressions (5.25),(5.27)-(5.29) which give the following relations:

$$K = -j\, k_o\sqrt{\epsilon_i}\, r \qquad (5.30)$$

$$Z_{ri} = \mathrm{Re}\left[-\frac{E_{\phi i}}{H_{yi}}\right] = \mathrm{Re}\left[\frac{Z_o}{\sqrt{\epsilon_i}}\right] \qquad i=1,2\ (\sqrt{\epsilon_2}=n) \qquad (5.31)$$

- which shows that far away from the interface, in the transverse direction, the two field components H_y and E_O form a plane wave propagating in a medium of relative permittivity ϵ_i

$$|H_y|^2 = \frac{c^2}{|K|}\exp\{2\mathrm{Re}[v\ \mathrm{arctanh}(K/v) - K] - 2\alpha_c R\phi)\}$$

which give the approximate relation for large radius and far away from the interface ($r\to\infty$):

$$|H_y|^2 = \frac{C^2}{k_o\sqrt{|\epsilon_i|}\,r}\, e^{\{2Re[jv\pi/2 - jk_o\sqrt{\epsilon_i}\,r] - 2\alpha z\}} \tag{5.32}$$

Finally the r-component of the Poynting vector:

$$S_r = \frac{1}{2}\frac{C^2}{\omega\epsilon_o|\epsilon_i|\,r}\, Re\left[\sqrt{\frac{|\epsilon_i|}{\epsilon_i}}\right] e^{\{Re[jv\pi - j2k_o\sqrt{\epsilon_i}\,r] - 2\alpha z\}} \tag{5.33}$$

for $i=1,2$ ($\epsilon_2=\epsilon_e$; $\sqrt{\epsilon_2}=n$ (3.19))

Note that this approximation is only valid for radius R large but finite. Indeed if R tends to infinity, (5.30) does not hold anymore but becomes:

$$K = k_i r = k_i R \tag{5.34}$$

and the effective impedance Z_{ri} (5.31) tends to zero in the lossless case (approximately equal to zero in the case of low loss).

Let us consider the case of Figure 6.b where R is large but less than r, r tends to infinity and small material loss is assumed. This leads to a complex propagation constant v with a small imaginary part that can be taken into account only in the exponent. Thus we have:

$$v=(\beta-j\alpha)R$$

where β and α are the propagation and attenuation constant computed for the plane interface case.

And

$$K=-jk_o\sqrt{\epsilon_1}\,r$$

Using the two above relations into (5.33) yields to:

$$S_{r1} = \frac{1}{2}\,\frac{c^2}{\omega\epsilon_o\epsilon_1 r}\,e^{\{\alpha\pi R - 2\alpha R\}} \tag{5.35}$$

In the case of Figure 6.a, we consider two different cases for the positive and negative real part of the effective dielectric constant:

If $\epsilon_e'>0$ then $n=n_R-jn_I$ (3.19) and

$$S_{r2} = \frac{1}{2}\,\frac{c^2}{\omega\epsilon_o\,|\epsilon_e|r}\,\mathrm{Re}\left[\sqrt{\frac{|\epsilon_e|}{\epsilon_e}}\right]\,e^{\{\alpha\pi R - 2kn_I r - 2\alpha z\}} \tag{5.36}$$

If $\epsilon_e'<0$ then $n=n_I-jn_R$ (3.19) and

$$S_{r2} = \frac{1}{2}\,\frac{c^2}{\omega\epsilon_o\,|\epsilon_e|r}\,\mathrm{Re}\left[\sqrt{\frac{|\epsilon_e|}{\epsilon_e}}\right]\,e^{\{\alpha\pi R - 2kn_R r - 2\alpha z\}} \tag{5.37}$$

I.4 Validity of the Bessel function approximation

When Debye's asymptotic expansions have been used in (5.5) to (5.8), only the first term of the expansion in 1/v has been taken into account. The relations derived are then valid only if all other terms can be neglected. This condition is satisfied if the second term of the series is negligible with respect to the first, i.e., [18,19]:

$$1/v\ (\ 1/8\ \text{cotanh}\ t - 5/24\ \text{cotanh}^3\ t\ ) << 1$$

where t is such that cosh t = v/x, with v the order and x the argument of the Bessel function involved. This yields:

$$\frac{1}{(24)^2}\ \frac{|2v^2 + 3x^2|^2}{|v^2 - x^2|^3} << 1$$

Such inequality is very general and may be used to test the validity of the results obtained. It is more interesting, however, to derive an expression giving the order of magnitude of the minimum radius acceptable. For such a purpose, the structure is asssumed to be lossless and is curved with a large radius such that $v = \beta R$. Furthermore, x is given by $x^2 = k_o^2 \epsilon_i r^2$, i=1,2 ($\epsilon_2 = \epsilon_e$) and evaluated at r=R since the approximations have to be valid in the vicinity of the interface (section I.2). Hence:

$$R >> \frac{1}{24}\ \frac{|2\beta^2 + 3K_o^2 \epsilon_i|}{|\beta^2 - k_o^2 \epsilon_i|^{3/2}} = R_{min} \qquad (5.38)$$

For the numerical examples of section 3.2.4, there results:

ω	β	100 R_{min} 1	100 R_{min} 2	$5/Re[k_i]$ 1	$5/Re[k_i]$ 2	$50\lambda_g$
10^{12}rad/s	rad/m	mm	mm	mm	mm	mm
2.4	19813	4.1	.9	.43	.29	16
2.2	16965	8.3	.1	.59	.25	18.5
1.5	10455	77.9	.4	1.7	.18	30

It is pointed out that at least 100 R_{min} is required for the asymptotic expansion to be valid within 1% accuracy.

VITA

Jean-Frederic Wagen, born on September 27, 1958, is a native of Lausanne, Switzerland. After receiving the Diplome d'Ingenieur Electricien from the Ecole Polytechnique Federale de Lausanne in January 1982, he undertook research in coupled microstripline analysis at the University College Dublin, Ireland. Subsequently, at the Centre National d'Etudes des Telecommunications in Lannion, France, he worked in speech analysis and synthesis. In September 1982, he joined the Department of Electrical and Computer Engineering at Lehigh University as a Teaching Assistant. From January 1983, he worked as a Research Assistant on the analysis of magnetoplasmons based near-millimeter wave structures. His research interests lie in the area of telecommunications including signal processing and microwaves.